V2 July 15

Filename: L drive TiO2 paper 6-4-15 with Sid comments draft 6.docx Paper [D] of the series

Differential genomic effects of six different TiO_2 nanomaterials on human liver HepG2 cells

Sheau-Fung Thai[a], Kathleen A. Wallace[a], Carlton P. Jones[a], Hongzu Ren[a], Eric Grulke[b], Benjamin T. Castellon[a], James Crooks[a], Kirk T. Kitchin[a]

[a]National Health and Environmental Effects Research Laboratory,

US Environmental Protection Agency, Research Triangle Park, NC, 27711 USA.

109 TW Alexander Dr., RTP NC 27711

[b]University of Kentucky, Department of Chemical & Materials

Engineering, Lexington, KY, 40506, USA

Corresponding Author:

Sheau-Fung Thai, PhD

thai.sheau-fung@epa.gov

Tel: 1-919-541-3942

Fax: 1-919-685-3229

Abstract

Engineered nanoparticles are reported to cause liver toxicity in vivo. To better assess the mechanism of the in vivo liver toxicity, we used the human hepatocarcinoma cells (HepG2) as a model system. Human HepG2 cells were exposed to 6 TiO_2 nanomaterials (with dry primary particle sizes ranging from 22 to 214 nm, either 0.3, 3 or 30 μg/ml) for three days. In culture media with 10% fetal bovine serum the hydrodynamic sizes ranged from 328 to 534 nm. With respect to physical-chemical characteristics, hydrodynamic agglomerated particle size rather than dry particle size or surface area correlated best with our biological and genomic outcomes. Even though all six NPs are composed of TiO2, they elicited fairly different canonical pathway responses. Some of these canonical pathways changed by nano-TiO_2 *in vitro* treatments have been already reported in literature, such as NRF2-mediated stress response, fatty acid metabolism, cell cycle and apoptosis, immune response, cholesterol biosynthesis and glycolysis. But this genomic study also revealed some novel effects such as protein synthesis, protein ubiquitination, hepatic fibrosis and cancer related signaling pathways. More importantly, this genomic analysis of HepG2 cells treated with 6 nano-TiO2 linked some of the *in vitro* canonical pathways to *in vivo* adverse outcomes, e.g., NRF2 mediated response pathways to oxidative stress, acute phase response to inflammation, cholesterol biosynthesis to steroid hormones alteration, fatty acid metabolism changes to lipid homeostasis alteration, G2/M cell checkpoint regulation to apoptosis and hepatic fibrosis/stellate cell activation to liver fibrosis. This study revealed some possible mechanisms through which nanoparticles caused liver toxicity in vivo.

Abbreviations: NP: nanoparticles; DEG: differentially expressed genes; FA: fatty acids; ROS: reactive oxygen species; IPA: Ingenuity Pathway Analysis.

Introduction

Titanium dioxide, TiO_2 nanoparticles (NPs) are among the most commonly used in consumer products, including paints, coatings, plastics, papers, inks, medications, pharmaceuticals, food products, cosmetics, sunscreens and toothpastes. Titanium dioxide nanoparticles (nano-TiO2) are also being used in additives in biomedical applications such as orthopedics, dental implants and drug delivery systems. Traditionally, nano-TiO_2 were considered non-toxic because larger sized (bulk) TiO_2 did not produce deleterious effects in previous toxicity tests [1]. However, there is increasing evidence suggesting that nanoparticles, particularly nano-TiO_2, pose a threat to human health.

Many *in vivo* studies show that NPs accumulate in the liver, kidney, spleen, lung, heart and brain; generate various inflammatory responses in mice [2]; and induce liver toxicity [3]. Intratracheal instillation of nano-TiO2 particles in rats demonstrates that a small fraction of nano-TiO_2 particles are transported from the airway lumen to the interstitial tissue and are subsequently released to the systemic circulation [4]. NPs accumulate in the liver after either intravenous or intraperitoneal injections of nano-TiO_2 in both mice [5-7] and rats [5-8]. After intravenous administration in mice, the liver had the highest accumulated amount of nanoparticles of all the tissues examined [5]. In one of the studies, liver damage was observed after intraperitoneal injection [9]The oral exposure route is important because nano-TiO_2 is widely used as a food additive, in toothpaste and capsules. Following oral exposure (single, high-dose gavage (5 g/kg) of

nano-TiO_2 in mice, nano-TiO_2 accumulated mainly in the liver and spleen [2]. There are many reports of nano-TiO_2 induced-toxicity to both the rodent respiratory tracts (in vivo) and *in vitro* lung cells [10, 11]. However, there are few reports on *in vitro* cytotoxicity on hepatocytes or *in vivo* liver toxicity.

The goal of the present *in vitro* dose-response study was to use genomic techniques to determine the signaling and canonical pathways altered by different nano-TiO_2 in human HepG2 cells. The design of our genomic studies emphasized nanomaterial toxicity, dose-response, structure-activity, the connection between physical-chemical properties and biological effects and also linking these effected genomic pathways to the *in vivo* adverse outcomes. New cellular targets of nano TiO_2 were sought. This *in vitro* information may also provide a possible molecular bases for predicting *in vivo* liver toxicity by these nanoparticles. This research is part of a large scale multi-disciplinary coordinated research program of the US EPA integrating different types of metal and metal oxide nanomaterials as stressors, different cells to represent expected target organs systems (e. g. lung, skin, gastrointestinal tract, liver, brain and eye), and types of biological responses (oxidative stress, inflammation etc.)[12-14]

Materials and Methods

Nanomaterials, their dispersion via ultrasound and their characterization

The six nano-TiO_2 used in this study (Supplementary Table I) were selected by the perceived data needs of the US EPA. These nanomaterials are being used by

multiple research laboratories at the US EPA in a coordinated research effort with many different scientific disciplines and experimental techniques [15].

The nanomaterials were obtained from five different vendors (Alfa Aesar, Degussa, NanoAmor (Nanostructured & Amorphous Materials, Inc.), Mknano and Acros). The chemical purity was high (> 98.8% for all cases and as high as 99.9% for five cases), the primary dry particle sizes ranged from 22 to 214 nm. With respect to crystal form, three of the TiO_2 nanomaterials contained both the anatase and rutile crystal forms (A, B and D); one contains only rutile (H), and the two other TiO_2 nanomaterials were all anatase (C and I).

All of the physical-chemical characterization and elemental composition analysis were done by Dr. Eric Grulke and his group at the University of Kentucky. Elemental analysis of nano-TiO2 was performed using ICP/MS (Plasma Quad 3 following EPA Method 200.7). Trace elements and Water, Solids and Biosolids analysis was performed using Inductively Coupled Plasma-Atomic Emission Spectrometry [16]. Specific surface area/porosity was measured using a Micromeritics TriStar BET. Crystal structure was assessed using a Siemens 5000 XRD. Particle shape and morphology were assessed with TEM and SEM. Supplemental Table I presents the six nanomaterials and their physical characterizations as dry powders. In the text of this paper the primary particle size presented is that from the University of Kentucky and not the vendors.

For dispersion of NPs, 0.01% (v/v) corn oil in PBS was added to dry nanomaterials in a glass vial. The general protein coating recipe of Dale Porter was

followed in that the ratio of the nanomaterial to BSA was 1/0.6 [17] Sonication was performed at a nanomaterial concentration of 3.34 mg/mL and 3.0 mLs of volume. Sonication was done for two 10 minute cycles of 13 seconds on, 7 seconds off with a typical total power of about 138 watts and 168,000 joules with a S-4000 Misonix Ultrasonic Liquid Processor with a 2.5 inch cup horn (Farmingdale, NY).

Excess unbound BSA and corn oil was removed by centrifuging (12,000 x g for 10 minutes) and resuspending the NPs in cell culture media. After nanomaterial dispersion, the degree of agglomeration was determined by dynamic light scattering at 35° C. Refractive index values for TiO_2 were 2.488 for anatase crystal structure, 2.609 for rutile crystal structure, 2.504 for the Degussa TiO_2 nanomaterial (86% anatase, 14% rutile from manufacturer's description). Size and zeta potential determinations were done both just after sonication and 3-days later to correspond with the end of cell exposure using a Malvern Model Zen3600 Zetasizer.

Chemical and cell culture methods

Chemicals and suppliers used in this study were: bovine serum albumin (Sigma, St. Louis, MO) and fetal bovine serum (Life Technologies, Grand Island, NY). Human Hepatocellular Carcinoma Cells, designation HepG2 (ATCC cat# HB-8065, Manassa, VA, USA) were obtained and expanded through passage seven using growth medium (Basal Medium Eagle, Gibco cat. 21010-046) containing 2mM GlutaMAX™ (Gibco cat.35050-061, Life Technologies), 1mM sodium pyruvate (Gibco cat. 11360-070, Life Technologies) and 10% fetal bovine serum and then frozen in liquid nitrogen. Cells

were subsequently carefully thawed and expanded before experimentation at passage number 10 to 20.

HepG2 is a human hepatocellular carcinoma cell line useful for many *in vitro* studies including polarized hepatocyte function, plasma protein secretion, liver metabolism, toxicity, genotoxicity and heptocarcinogenesis. Cell cultures were maintained in a humidified incubator at 37°C and 95%Air/5% CO_2 during the study. Cells were plated at 40,000 cells/cm^2 in vented T-25 flasks (Corning) for 48 hours prior to nanomaterial exposure. Working stocks of each nanomaterial were prepared at 1.0 mg per mL and diluted using culture medium. Individual flasks were dosed with 200 uL per cm^2 of the appropriate nanomaterial dilution, and incubated for 72 hours. At the end of 72 hours, the media was vacuum aspirated and the flasks rinsed with warm Dulbecco's Phosphate-Buffered Saline (DPBS). RNA was extracted following procedure described in "RNA extraction".

Cytotoxicty assays and kits

Many common cytotoxicity assays (MTT (3-[4,5-dimethyl-2-thiazol]-2,5-diphenyl-2H-tetrazolium bromide, CAS 298-93-1, (Sigma-Aldrich, St Louis, MO)), MTS (4-[5-[3-(carboxymethoxy)phenyl]-3-(4,5-dimethyl-1,3-thiazol-2-yl)tetrazol-3-ium-2-yl]benzenesulfonate, CAS 138169-43-4, (Promega, Madison, WI)), alamar blue (resazurin, CAS 62758-13-8, (Cell Tier-Blue, Promega, Madison, WI)), neutral red (3-amino-7-dimethylamino-2 methylphenazine hydrochloride, CAS 553-24-2, (Sigma-Aldrich, St Louis, MO)), ATP (Promega, Madison, WI) and simple visual examination of the cells) have been used by our laboratory seeking to avoid or minimize interferences

from the study nanomaterials themselves. After 3 days of culture with various nanomaterials, cytotoxicity assays based on MTT, MTS, alamar blue and ATP were performed using the assay kit directions. Neutral red (Sigma-Aldrich, St Louis, MO) uptake cytotoxicity assays were also performed. Cytotoxicity assays results were always checked with each other and with visual assessment of the cells to ensure the cytotoxicity assays were working well.

RNA extraction

Total RNA was extracted from cells using a mirVana™ RNA extraction kit (Life Technologies, Grand Island, NY) following the manufacturer's protocol. In short, cells were lysed with lysis buffer. RNA was extracted by acid phenol-chloroform, then precipitated with ethanol and purified through glass fiber columns. RNA integrity was assessed by the RNA 6000 LabChip® kit using a 2100 Bioanalyzer (Agilent Technologies, Palo Alto, CA). The RNA Integrity number (RIN) of all samples were between 9.8 and 10.0.

Microarray analysis, statistical analysis and pathway analysis

The global gene expression change was analyzed by using Illumina Human HT-12 v4 Expression Beadchips following the manufacturer's protocol. This version of Illumina Human HT BeadChips targets more than 47,000 transcripts derived from NCBI Reference Release 38. The data processing was performed using Bioconductor's

beadarray package (version 2.4.1) for the R language (version 2.14.0). The bead-level data were loaded into a single data object using the *readIllumina* function and a log2 transformation of the intensity data was performed. A probe-level summary was produced using the *summarize* function by taking the median log2-intensity for each bead-type. A quantile normalization of this probe-level data was performed using the *normaliseIllumina* function. The *illuminaHumanv4.db* package (version 1.12.1) containing the Illumina HumanHT12v4 annotation data was used to annotate the normalized probe-level data.

Statistical analysis was performed using R's *limma* package (version 3.10.0). First, a matrix encoding the contrasts between all 24 treatment categories and the control was created. The 1-way ANOVA analysis was performed on all probes using the *lmFit* function, and the estimated variances of the probes were regularized using the *eBayes* function. A list of the most differentially expressed probes (genes) for each contrast was generated using the *topTable* function. To correct for multiple comparisons, only those probes with both a Benjamini-Hochberg corrected p-value of less than 0.05 and a 1.5x or greater fold change were placed on the DEG list. Statistically significant gene changes in each dose group were analyzed in terms of their associated molecular/cellular functions and inclusion in canonical pathways using Ingenuity Pathway Analysis (IPA, v1485783, release date 4-30-2013, Ingenuity Systems, Redwood City, CA).

Results

Nanoparticle properties

The NPs evaluated in this study were characterized by the vendor and the University of Kentucky. All the NPs have the same chemical composition, TiO2, but differ in crystal structure, the ratio of anatase and rutile, size of the particle, purity and surface areas. Fuller physical-chemical characterization of TiO_2 nanomaterials D and H are given in Supplemental Table 1 and in Supplemental information 1. Physical-chemical characterization of TiO_2 nanomaterials A, B, C and I have been published elsewhere [18]. The hydrodynamic agglomerated nanoparticle sizes and zeta potentials measured at time 0 and 72 hours are listed in Table 1.

Cytotoxicity

Cytotoxicity was determined using assays to evaluate multiple endpoints (MTS, MTT, alamar blue, ATP, visual examination of cells, cellular microalbumin and protein, and also release of the enzymes LDH, ALT and AST). At 0.3 and 3 μg/ml there was no cytotoxicity (Kitchin et al, manuscript submitted to JNN). At 30 μg/ml NPs A, H and I did not produce cytotoxicity, but B, C and D produced a cytotoxic response. At 300 and 1000 μg/ml, all of these TiO_2 NPs produced cytotoxicity. The order of decreasing cytotoxicity for these TiO_2 NPs was C > D > B > H, I > A (Kitchin et al., in preparation). These cytotoxicity results roughly correlates with surface area of the NPs as C and D have the largest surface areas while H and I have the smallest.

Differentially Expressed Genes (DEG) and Dose-response

The number of DEGs from each treatment is listed in Table 2. The number of genes altered by 30 μg/ml nano-TiO_2 treatment (D< C< H< I< A <B) roughly correlated with the agglomerated particle sizes rather than the dry particle sizes. At 30 μg/ml, the

mean hydrodynamic particle sizes were 328 (D), 331 (C), 403 (A), 453 (H), 468 (I) and 534 nm (B). All of the nano-TiO_2 treatments resulted in a monotonic dose-response except nano H. Nano H treatments resulted in more genes being changed in lowest dose (397 genes) than of higher doses (158 at 3 μg/ml and 241 at 30 μg/ml). We repeated nano H treatments and gene profiling experiments and obtained similar results (data not shown). Thus, the results with nano H are repeatable. [20]

Ingenuity Pathway Analysis (IPA)

The differentially expressed genes from each treatment were evaluated using Ingenuity Pathway Analysis (IPA) to delineate the canonical/signaling pathways changes. The15 canonical pathways with lowest p values altered by each nano-TiO_2 at 30 μg/ml are listed in Table 3; since low dose nano H (0.3 ug/ml) caused more canonical pathway changes than the high dose, we included it in the table.

Discussion

Dose-response

Four of the TiO_2 nanomaterials produced monotonic dose-response effects in the number of DEGs (A, B, C and D) (Table 2). For example, nano C produced 10, 25 and 228 DEGs at 0.3, 3 and 30 μg/ml, respectively. However, both H and I gave dose-response relationships that did not display much positive slope over a 100-fold increase in exposure concentration (397, 158 and 241 DEGs for H and 323, 480, 479 for I at 0.3, 3 and 30 μg/ml, respectively). The observation of unexpectedly high number of DEGs

at low doses has been observed before both in our genomic work and the work of others [20], [25]. In addition to the size of the aggregates, there are other properties that affect the properties of these NPs, e.g., chemical composition, impurities in the preparations, size and surface area, shape, crystal structure, inherent activity of the surfaces, coating with proteins, lipids and other cell culture conditions. The nano-TiO_2 NPs used have the same chemical composition (all are TiO_2), but they have different dry particle sizes, crystal structures, surface areas, and agglomeration properties and could have different protein composition in the protein corona. All these different factors can contribute to the effects of the NPs on the gene expression and toxicity. It points out the value of repeating such low exposure concentrations to test the reproducibility of these unexpected low dose results and of extending the experimentation to even lower doses that might also exhibit some biological activity.

Dry particle size, hydrodynamic agglomerated particle sizes and endocytosis

All six nano-TiO2 agglomerated under the protein and corn oil coating, ultrasonication dispersion and culture media conditions (with 10% fetal bovine serum) we employed, an observation that is consistent with literature [26]. As the NP concentration increases, the hydrodynamic agglomerated NP sizes determined on day 0 of culture also increase (looking at Size by Peak). However, after incubating in the culture media for 3 days, the agglomerated sizes at high concentration became smaller (comparing size at 0 hour and 72 hour) with nano A being the only exception. The reason for reduction in the agglomerated sizes are not clear, some possible reasons

may be settling, absorption to the surface of the culture flask and endocytosis of the larger particles. The hydrodynamic agglomerated sizes did not correlate with the dry primary particle size of the NPs. The literature has indicated that the hydrodynamic agglomerated NP sizes to which the cells are exposed are important and affect biological properties such as cellular absorption, cytotoxicity and gene expression profiles [19, 27]. Our results are consistent with the literature. At 30 μg/ml the order of size of hydrodynamic agglomerated NP are B > I ≥ H > A > C ≥ D (Table 1). At 30 μg/ml, the order of altered genes is B > A > I > H ≥ C > D. Thus for these NPs the # of DEGs roughly follows the hydrodynamic agglomerated sizes at day 0 and not the dry primary particle sizes or the surface areas. This indicates that the hydrodynamic agglomerated sizes may be one of the more important factors in both determining the cellular uptake and subsequently the biological properties affected by the NPs

Nanoparticles are taken into cells through endocytosis and then can alter the gene expression profiles. We believe that alterations in the gene expression levels (either up- or down-regulation) in a particular signaling pathway indicate the deviation from the homeostasis as a result of the NP treatment. There is a tendency of getting everything back to homeostasis, and depending on the time we look at the gene expression, it could be up- or down-regulated. There are three major endocytosis pathways, caveolar-mediated endocytosis, clathrin-mediated endocytosis and macropinocytosis. Expression of genes in all three endocytosis pathways are altered by nano B (Table 4) indicating a change in homeostasis caused by NP treatment. Clathrin-mediated endocytosis genes are altered in nano B, I and H high doses, while caveolar-mediated endocytosis is altered in nano A and B high dose treated cells. Both clathrin-

and caveolar-mediated endocytosis are altered in multiple nano-TiO2 treated cells. But macropinocytosis was only altered in nano B high dose treated cells. This is consistent with the agglomerated sizes of the NPs. Nano B is the only one that has an agglomerated size (at day 0) larger than 500 nm which is the average size necessary for macropinocytosis to take place.

Connecting physical-chemical characteristics and biological outcomes

In earlier observations from our TiO_2 and CeO_2 research, GSH depletion may correlate somewhat with smaller dry particle size and larger surface area [18]. Of the four nano-TiO2 that analyzed by metabolomics, only nanomaterials A, B and C which have the smaller dry particle sizes caused reduction in the HepG2 GSH levels, while nanomaterial I did not.

In contrast, most of the DEGs results of this study showed good correlation between hydrodynamic size and biological potency. When the number of DEGs is divided by the hydrodynamic diameter, numbers ranging from 0.51 to 2.58 result (Table 3). In other words all the TiO_2 nanomaterials acted roughly with the same potency per wet size. In contrast, if the number of DEGs is divided by the dry surface area, a much larger range of values results (from 1.9 to 68.5) (Table 3), suggesting a poor correlation between dry surface area and DEGs. Theoretically, many biological outcomes should be roughly proportional to nanomaterial surface area and the cells are exposed to the hydrodynamic diameter of the agglomerated nanomaterials not the dry particle diameter.

Canonical pathways

In order to demonstrate that there are some pathways that may be important in understanding the effects of these NPs on the HepG2 cells but not present in Table 3, we chose some relevant categories of effects and listed the rank of pathways altered in IPA (Table 4). It is clear from table 4 that there are common pathways that are altered by more than one nano-TiO_2, such as EIF2 signaling (altered by 4 out of 6 NPs), acute phase response signaling (altered by 3 NPs) and others. There are also pathways that are only altered by one nano-TiO_2, such as hepatic fibrosis/hepatic stellate cell activation for nano D and FXR/RXR signaling for nano B.

A. Stress response

There is at least one stress response pathway altered in all the NP treated HepG2 cells except nano C treatment (Table 4).

1. Mitochondrial dysfunction and fatty acid metabolism

Mitochondrial dysfunction is only significantly altered in nano H low dose. In addition to nano H, fatty acid activation, FA beta-oxidation and L-carnitine shuttle pathways (all three pathways involve in fatty acid oxidation) are also affected in nano I, D and C treated cells.

The observed effects of these nano particles on mitochondria and the lipid homeostasis *in vitro* are consistent with literature. Metal oxide nanoparticles have been shown to cause changes in lipid metabolism and mitochondrial membrane potential imbalance *in vitro* [28-31] and *in vivo* [3, 7, 32, 33]. Changes in mitochondrial redox state, membrane potential and intracellular calcium levels precede mitochondrial dysfunction. Our group

also observed fatty acids accumulation [18] and mitochondrial dysfunction following nano-CeO_2 exposure in HepG2 cells.

2. NRF2-mediated stress response

The NRF2-mediated stress response was altered only in A and B, the two with the highest GSH concentration reduction. The nano A high dose upregulated most of the genes downstream of NRF2 in this pathway, e.g., HSP90, AOX1, STIP1 and TRXR1 (Supplemental Table 2). MAFG, which heterodimerizes with NRF2 to bind to the antioxidant response element (ARE), is upregulated in nano A high dose treated cells. Thus, there is a strong indication that the NRF2-mediated stress response is upregulated in these cells. As a result, these cells could be protected from the ROS insults by the induction of antioxidant enzymes. However, in the nano B treated cells, some of the down-stream genes in this pathway are downregulated, while others are upregulated. Therefore, whether the NRF2-mediated stress response pathway is up- or downregulated cannot be easily determined from genomic data. ROS production, reduced levels of GSH and perturbation of GSH redox reaction in the liver *in vivo* after nano-TiO2 treatment has been reported [9, 34, 35] but alteration of the NRF2-mediated stress response has only been reported in the nano TiO_2 treated brain microglia [36]. Our results show that not all of the nano TiO_2 altered the NRF2 signaling pathway. Nano A (Degussa P25) induced NRF2-mediated stress response in brain microglia cells [36] and also induced NRF2 signaling in our HepG2 cells. The six NPs used in this study were reported to cause DNA-centered free radical formation in a cell free system, and all of them were shown to increase ROS production in that system, albeit at varying

degrees of potency [15]. These results taken together clearly point to differential effects of these nano-TiO_2 on ROS response in HepG2 cells.

3. Acute phase response signaling

The acute phase response is a rapid non-specific inflammatory response that provides defensive protection against microorganisms, tissue injury, trauma or surgery. After a single stimulus the levels of these proteins remain elevated for at least 24 hours and decrease after about 48 hours [37]. Acute phase response was reported to be induced by nano-TiO2 in the lung of treated mice [38]. In the liver, key players in the acute phase response are pro-inflammatory cytokines, particularly, IL-1, IL-6 and TNFα. *In vivo* studies have shown that nano TiO_2 caused upregulation of IL-1, IL-6 and TNFα expressions both at mRNA and protein levels [3], an indication of altered acute phase response. Acute phase response is changed in nano H high and low, and in nano B and I high dose treated cells. IL-1RN, an IL-1 receptor antagonist, is downregulated in both nano I and H high dose. Most of the altered genes in this pathway are upregulated in nano I and H high dose treated cells, indicating an induction of acute phase response signaling in these cells. However, IL-1RN is upregulated in nano B high and H low dose treated cells, indicating a downregulation of this signaling pathway. So, two of the six nano TiO2 up-regulated and two down-regulated inflammatory response in HepG2 cells.

4. Hepatic fibrosis/hepatic stellate cell activation

Early stage of hepatic fibrosis was observed in mice treated with a nano TiO_2 (3.6 nm) by intraperitoneal injection [5]. The fibrosis signaling pathway is only altered in nano D

high dose treated cells. Both downregulated genes IGFBP4 [39] and SERPINE 1 (also known as plasminogen activator inhibitor 1, PAI-1) are fibrogenic. Of the two upregulated genes, IL-10 is antifibrogenic, [40], while Leptin is fibrogenic (Supplemental Table 2). With more antifibrogenic genes upregulated and fibrogenic genes downregulated nano D high dose treated cells appear less likely to cause fibrosis. However, these results were from *in vitro* treatments, and *in vivo* studies are needed to more strongly support or refute these nano D effects.

There are many reports on negative effects on hepatic functions, e.g., altered ALT/AST, inflammation, apoptosis and more [41], but there is only one group that reported observed hepatic fibrosis in mice 14 days after nano-TiO2 treatment [5], showing the need of more animal studies in this area. Five out of six NPs in present study caused some kind of stress response. Nano C is the only NP that did not induce any of the stress response pathways listed in Table 4 in the present genomics study. However, in the metabolomics study, nano C did reduce GSH level to 34% of the control level.

B. Cell cycle and apoptosis

Nano TiO_2(various sizes and forms) have been shown to be genotoxic and cause both DNA damage and apoptosis in HepG2 cells [34, 35] and *in vivo* mouse liver [10], possibly as a result of ROS generation. DNA damage triggers disturbances in G2/M cell cycle checkpoint regulation. G2/M cell cycle checkpoint regulation was affected in nano B, D and I treated cells. All three of three NPs are higher in anatase than rutile crystal form, and this is consistent with reports that anatase is more active of the two crystal

forms. Moreover, these three nano TiO_2 are the three with the largest particle sizes of anatase form. Whether the particle sizes play a part in causing G2/M DNA damage checkpoint regulation awaits further research.

All of the genes pertaining to the G2/M cell cycle checkpoint pathway in cells treated by nano I (7 genes) and D (2 genes) respectively, were downregulated. That indicated these cells were slowed down as they proceeded through this checkpoint (Supplemental Table 2). In nano B treated cells cell cycle seems disturbed because ATM is upregulated and other affected genes in cell cycle progression such as CDC2 are upregulated, thus these cells are likely to experience some cell cycle disturbance at the G2/M checkpoint. This interpretation also awaits further studies to confirm or refute it. This is consistent with the cytotoxicity data which showed some cell death for nano B high dose, but very little death for nano D and I.

C. Immune response

Inflammatory response is reported in nano-TiO2 treated mice [3]. In our *in vitro* system, the complement system (altered in B and H high treatments) and IL-3, IL-4 and IL-5 signaling pathways (altered in the H low treatment) are the only inflammation-related pathways altered besides acute response signaling. Therefore, inflammatory/immune response pathways are not strongly altered by nano-TiO2 in our HepG2 cells. It is reported that liver reticuloendothelial Kupffer cells are much more responsive to inflammatory stimulation than are hepatocytes [42], this may explain why we did not see a strong immune response in HepG2 cells (originated from hepatocytes).

D. Metabolism

Protein synthesis/degradation

Protein synthesis is not presently known to be altered by NPs *in vivo*. However, many protein synthesis genes are altered by most of the TiO_2 NPs in our *in vitro* study. Nano A, B I, and H (both high and low) treatments affected expression of genes related to translation initiation, EIF2 signaling, mTOR signaling and regulation of eIF4 and p70S6K signaling while nano D and C did not. Genes in these four pathways do not show a consistent pattern of up- or down-regulation, therefore, it is hard to determine how these NPs affect these pathways. Another pathway related to protein modification is the protein ubiquitination pathway. Protein ubiquitination effects happened only in nano B, D and I treated cells. Nano B, D and I have anatase form and larger particle sizes. Our group also observed alteration of these pathways in nano CeO_2 treated HepG2 cells (Thai et al. submitted to Nanoscience and Nanotechnology). These results are again pointing to the complexity of the cellular responses to the NP treatments.

NPs have been shown to react with cellular molecules, including proteins. The NPs that affected protein synthesis are different from the NPs that affected protein ubiquitination, indicating different mechanisms are employed.

Glycolysis and cholesterol biosynthesis

Nanoparticles effects on glycolysis in cultured cells and in mice have been reported [7, 43] and our group also observed similar results from nano CeO_2 treated HepG2 cells (Thai et al, accepted by JNN). Glycolysis is affected in nano A and I high dose treated cells and most of the affected genes are downregulated indicating a slowed or lower production of pyruvate from this pathway.. However, genes in the TCA cycle are not affected by these NPs treatments. Cholesterol biosynthesis and FXR/RXR signaling, which regulates cholesterol metabolism, are affected only in nano B high dose treated cells while bile acid biosynthesis and zymosterol (a precursor of cholesterol) biosynthesis are affected only in nano A and D high dose treatments (Supplemental Table 2). Liver is the major organ for cholesterol synthesis in animals, therefore, this cholesterol biosynthesis effect of NPs may have systemic and long term effects on the whole animal. Since cholesterol is essential for the structure and function of caveolae- and clathrin-coated pits, endocytosis process may be affected by nanoparticle treatments. Cholesterol is also a precursor for vitamin D and steroid hormones including sex hormones. The alteration in metabolism of cholesterol may affect vitamin D and other hormones down-stream of cholesterol. Nanoparticle induced alteration of cortisol and sex hormone have been reported in rodent models [44, 45].

E. Cancer related signaling pathways

BulkTiO_2 is not carcinogenic to humans [46] or to rats or mice in feeding studies (NTP, 1979). However, nano-TiO_2 can produce lung tumors in rats when exposed through inhalation or intratracheal instillation [47]. Even though no liver cancer has

been reported in animal treated with nano-TiO2, oxidative stress and DNA damage (cancer precursor events) have been reported in the livers of the treated animals [23, 48]. Hepatic fibrosis was observed in the liver after intraperitoneal injection of 1.94 g/kg of nano TiO_2 in mice [5]. While liver fibrosis itself is benign, it may progress to liver cirrhosis and may eventually cause liver cancer. The liver is a major accumulation organ after TiO_2 exposure [2, 5]. In the present study we report that the nano TiO_2 also induces different cancer signaling pathways in HepG2 cells. In combination, these data point to the need for more studies on the carcinogenesis potential for nano TiO_2 in animals.

Conclusions:

We used six TiO_2 NPs differing in size and crystal structures to treat HepG2 cells and performed genomic studies to identify altered genes/signaling pathways. The results show: 1) the potency of the NPs to alter gene expression correlates better with the hydrodynamic agglomerated size rather than the dry primary particle size, 2) even though all six NPs have the same elemental composition, they elicited quite different responses/canonical pathways in HepG2 cells, 3) nano-TiO_2 altered canonical pathways which have been reported in literature from *in vitro* studies, such as NRF2-mediated stress response, fatty acid metabolism and glycolysis, 4) some novel pathways such as protein synthesis, protein ubiquitination, hepatic fibrosis and cancer related signaling pathways were not reported before in any of the *in vitro* studies, 5) many canonical pathways altered by nano-TiO_2 *in vitro* treatments correlated well with

the *in vivo* toxicological changes such as inflammation, oxidative stress, lipid metabolism, cholesterol biosynthesis, G2/M cell cycle checkpoint regulation and hepatic fibrosis, 6) with the exception of H and I, these six nano-TiO_2 nanomaterials gave monotonic dose-response relationship from 0.3 to 30 μg/ml, and 7) connecting physical-chemical characteristics with biological outcomes is difficult because of the large number of physical-chemical parameters that may determine the biological effects. In spite of this limitation we have been able to make some general observations correlating biological effects with hydrodynamic agglomerated particle size, dry particle size and surface area.

Acknowledgements: This paper is a product of the NHEERL nano-materials research team. Dr. Kevin Dreher managed the US EPA contract that resulted in physical-chemical characterization of some TiO_2 and CeO_2 nanomaterials. We also thank our colleagues, Drs. Laura Degn and Gail Nelson, and Sid Hunter who reviewed this manuscript for EPA's in house prepublication clearance.

Declaration of interest:

The authors declare that they have no potential conflicts of interest.

Disclaimer:

The information in this document has been funded wholly by the U. S.

Environmental Protection Agency. It has been subjected to review by the National Health and Environmental Effects Research Laboratory and approved for publication. Approval does not signify that the contents necessarily reflect the views of the Agency, nor does mention of trade names or commercial products constitute endorsement or recommendation for use.

List of tables

References

1. Heinlaan, M., et al., *Toxicity of nanosized and bulk ZnO, CuO and TiO2 to bacteria Vibrio fischeri and crustaceans Daphnia magna and Thamnocephalus platyurus.* Chemosphere, 2008. **71**(7): p. 1308-16.
2. Wang, J., et al., *Acute toxicity and biodistribution of different sized titanium dioxide particles in mice after oral administration.* Toxicol Lett, 2007. **168**(2): p. 176-85.
3. Ma, L., et al., *The Acute Liver Injury in Mice Caused by Nano-Anatase TiO2.* Nanoscale Res Lett, 2009. **4**(11): p. 1275-85.
4. Muhlfeld, C., et al., *Re-evaluation of pulmonary titanium dioxide nanoparticle distribution using the "relative deposition index": Evidence for clearance through microvasculature.* Part Fibre Toxicol, 2007. **4**: p. 7.
5. Chen, J., et al., *In vivo acute toxicity of titanium dioxide nanoparticles to mice after intraperitioneal injection.* J Appl Toxicol, 2009. **29**(4): p. 330-7.
6. Li, Y., et al., *Systematic influence induced by 3 nm titanium dioxide following intratracheal instillation of mice.* J Nanosci Nanotechnol, 2010. **10**(12): p. 8544-9.
7. Liu, H., et al., *Biochemical toxicity of nano-anatase TiO2 particles in mice.* Biol Trace Elem Res, 2009. **129**(1-3): p. 170-80.
8. Fabian, E., et al., *Tissue distribution and toxicity of intravenously administered titanium dioxide nanoparticles in rats.* Arch Toxicol, 2008. **82**(3): p. 151-7.
9. Jeon, Y.M., W.J. Kim, and M.Y. Lee, *Studies on liver damage induced by nanosized-titanium dioxide in mouse.* J Environ Biol, 2013. **34**(2): p. 283-7.
10. Chang, X., et al., *Health effects of exposure to nano-TiO2: a meta-analysis of experimental studies.* Nanoscale Res Lett, 2013. **8**(1): p. 51.
11. Christensen, F.M., et al., *Nano-TiO(2)--feasibility and challenges for human health risk assessment based on open literature.* Nanotoxicology, 2011. **5**(2): p. 110-24.
12. Boyes, W.K., et al., *The neurotoxic potential of engineered nanomaterials.* Neurotoxicology, 2012. **33**(4): p. 902-10.
13. Prasad, R.Y., et al., *Effect of treatment media on the agglomeration of titanium dioxide nanoparticles: impact on genotoxicity, cellular interaction, and cell cycle.* ACS Nano, 2013. **7**(3): p. 1929-42.
14. Thai, S., KA Wallace, CP Jones, H Ren, RY Prasad, WO Ward, MJ Kohan, CF Blackman, *Signaling pathways and microRNA changes in nano-TiO2 treated human lung epithelial (BEAS-2B) cells.* Journal of nanoscience and nanotechnology, 2015. **15**: p. 492-503.
15. Kitchin, K.T., R.Y. Prasad, and K. Wallace, *Oxidative stress studies of six TiO(2) and two CeO(2) nanomaterials: immuno-spin trapping results with DNA.* Nanotoxicology, 2011. **5**(4): p. 546-56.
16. Martin, T.D., C.A. Brockhoff, J.T. Creed and E.M. W. Group, *Determination of metals and trace elements in water and waste by inductively coupled plasma-atomic emission spectrometry. Revision 4.4.* EPA method, US EPA, Cicinnati, OH, 1994. **200.7**.
17. Porter, D., Sriram, K., Wolfarth, M., Jefferson, A., Schwegler-Berry, D., Andrew, M., & Castranova, V., *A biocompatible medium for nanoparticle dispersion.* Nanotoxicology, 2008. **2**(3): p. 144-154.
18. Kitchin, K.T., E. Grulke, B. L. Robinette and B. T. Castellon, *Metabolomic effects in HepG2 cells exposed to four TiO2 and two CeO2 nanomaterials.* Environmental Science Nano, 2014. **1**: p. 466-477.
19. Okuda-Shimazaki, J., et al., *Effects of titanium dioxide nanoparticle aggregate size on gene expression.* Int J Mol Sci, 2010. **11**(6): p. 2383-92.
20. Iavicoli, I., E.J. Calabrese, and M.A. Nascarella, *Exposure to nanoparticles and hormesis.* Dose Response, 2010. **8**(4): p. 501-17.
21. Ory, D.S., *Nuclear receptor signaling in the control of cholesterol homeostasis: have the orphans found a home?* Circ Res, 2004. **95**(7): p. 660-70.
22. Cui, Y., et al., *Gene expression in liver injury caused by long-term exposure to titanium dioxide nanoparticles in mice.* Toxicol Sci, 2012. **128**(1): p. 171-85.
23. Trouiller, B., et al., *Titanium dioxide nanoparticles induce DNA damage and genetic instability in vivo in mice.* Cancer Res, 2009. **69**(22): p. 8784-9.

24. Kang, M.C., et al., *Protective effect of a marine polyphenol, dieckol against carbon tetrachloride-induced acute liver damage in mouse.* Environ Toxicol Pharmacol, 2013. **35**(3): p. 517-23.
25. Nascarella, M.A. and E.J. Calabrese, *A method to evaluate hormesis in nanoparticle dose-responses.* Dose Response, 2012. **10**(3): p. 344-54.
26. Zhou, D., et al., *Influence of material properties on TiO2 nanoparticle agglomeration.* PLoS One, 2013. **8**(11): p. e81239.
27. Levina, A., et al., *Nanocomposites consisting of titanium dioxide nanoparticles and oligonucleotides.* J Nanosci Nanotechnol, 2012. **12**(3): p. 1812-20.
28. Siddiqui, M.A., et al., *Copper oxide nanoparticles induced mitochondria mediated apoptosis in human hepatocarcinoma cells.* PLoS One, 2013. **8**(8): p. e69534.
29. Xia, T., et al., *Comparison of the abilities of ambient and manufactured nanoparticles to induce cellular toxicity according to an oxidative stress paradigm.* Nano Lett, 2006. **6**(8): p. 1794-807.
30. Huang, C.C., et al., *Oxidative stress, calcium homeostasis, and altered gene expression in human lung epithelial cells exposed to ZnO nanoparticles.* Toxicol In Vitro, 2010. **24**(1): p. 45-55.
31. Sharifi, S., et al., *Superparamagnetic iron oxide nanoparticles alter expression of obesity and T2D-associated risk genes in human adipocytes.* Sci Rep, 2013. **3**: p. 2173.
32. Duan, Y., et al., *Toxicological characteristics of nanoparticulate anatase titanium dioxide in mice.* Biomaterials, 2010. **31**(5): p. 894-9.
33. Hussain, S.M., et al., *In vitro toxicity of nanoparticles in BRL 3A rat liver cells.* Toxicol In Vitro, 2005. **19**(7): p. 975-83.
34. Petkovic, J., et al., *DNA damage and alterations in expression of DNA damage responsive genes induced by TiO2 nanoparticles in human hepatoma HepG2 cells.* Nanotoxicology, 2011. **5**(3): p. 341-53.
35. Shukla, R.K., et al., *TiO(2) nanoparticles induce oxidative DNA damage and apoptosis in human liver cells.* Nanotoxicology, 2013. **7**(1): p. 48-60.
36. Long, T.C., et al., *Nanosize titanium dioxide stimulates reactive oxygen species in brain microglia and damages neurons in vitro.* Environ Health Perspect, 2007. **115**(11): p. 1631-7.
37. Gruys, E., et al., *Acute phase reaction and acute phase proteins.* J Zhejiang Univ Sci B, 2005. **6**(11): p. 1045-56.
38. Halappanavar, S., et al., *Pulmonary response to surface-coated nanotitanium dioxide particles includes induction of acute phase response genes, inflammatory cascades, and changes in microRNAs: a toxicogenomic study.* Environ Mol Mutagen, 2011. **52**(6): p. 425-39.
39. Boers, W., et al., *Transcriptional profiling reveals novel markers of liver fibrogenesis: gremlin and insulin-like growth factor-binding proteins.* J Biol Chem, 2006. **281**(24): p. 16289-95.
40. Zhang, L.J., et al., *Antifibrotic effects of interleukin-10 on experimental hepatic fibrosis.* Hepatogastroenterology, 2007. **54**(79): p. 2092-8.
41. Iavicoli, I., V. Leso, and A. Bergamaschi, *Toxicological effects of titanium dioxide nanoparticles: a review of in vivo studies.* J. of Nanomaterials, 2012.
42. Zimmermann, H.W., C. Trautwein, and F. Tacke, *Functional role of monocytes and macrophages for the inflammatory response in acute liver injury.* Front Physiol, 2012. **3**: p. 56.
43. Tucci, P., et al., *Metabolic effects of TiO2 nanoparticles, a common component of sunscreens and cosmetics, on human keratinocytes.* Cell Death Dis, 2013. **4**: p. e549.
44. Li, C., et al., *Effect of nanoparticle-rich diesel exhaust on testosterone biosynthesis in adult male mice.* Inhal Toxicol, 2012. **24**(9): p. 599-608.
45. Yamagishi, N., et al., *Effect of nanoparticle-rich diesel exhaust on testicular and hippocampus steroidogenesis in male rats.* Inhal Toxicol, 2012. **24**(8): p. 459-67.
46. Fryzek, J.P., et al., *A cohort mortality study among titanium dioxide manufacturing workers in the United States.* J Occup Environ Med, 2003. **45**(4): p. 400-9.
47. Borm, P.J., R.P. Schins, and C. Albrecht, *Inhaled particles and lung cancer, part B: paradigms and risk assessment.* Int J Cancer, 2004. **110**(1): p. 3-14.
48. Shi, H., et al., *Titanium dioxide nanoparticles: a review of current toxicological data.* Part Fibre Toxicol, 2013. **10**: p. 15.

table 1

Nanoparticle ID	A														
Time	0 hour									72 hour[a]					
Type of DLS Characterization	Size by Peak[b]		Size by Z-Average[c]				Zeta Potential			Size by Peak		Size by Z-Average				Zeta Potential
	Mean (nm)	SEM[d]	Mean (nm)	SEM	Mean PdI[e]	N[f]	Mean (mV)	SEM	N	Mean (nm)	SEM	Mean (nm)	SEM	Mean PdI	N	Mean (mV)[g]
Media with 10% FBS[h]	23.7	3.2	15.7	0.6	0.33	3	-2.4	1.00	3	133.1	23.9	259.1	47.5	0.32	3	-8.58
0.3 µg/ml	159.2	10.9	214.4	22.8	0.27	3	-8.9	0.15	3	171	3.5	138.4	5.1	0.46	3	-8.48
3 µg/ml	218.1	2.5	211.6	7.6	0.25	3	-10.8	0.60	3	241.4	16.4	194.3	10.6	0.47	3	-8.83
30 µg/ml	402.8	17.3	356.5	7.4	0.38	3	-10.1	0.52	3	423.1	27.6	345.0	2.4	0.38	3	-9.79

Nanoparticle ID	B														
Time	0 hour									72 hour					
Type of DLS Characterization	Size by Peak		Size by Z-Average				Zeta Potential			Size by Peak		Size by Z-Average				Zeta Potential
	Mean (nm)	SEM	Mean (nm)	SEM	Mean PdI	N	Mean (mV)	SEM	N	Mean (nm)	SEM	Mean (nm)	SEM	Mean PdI	N	Mean (mV)
Media with 10% FBS	23.7	3.2	15.7	0.6	0.33	3	-2.4	1.00	3	133.1	23.9	259.1	47.5	0.32	3	-8.58
0.3 µg/ml	68.9	24.2	1345	366.9	0.81	3	-9	1.08	3	143.9	4.7	225.9	8.3	0.29	3	-9.7
3 µg/ml	191.4	7.1	1141	78.8	0.83	3	ND[i]			150.4	13.7	489.9	61.3	0.54	3	-8.8
30 µg/ml	534	17.1	726.0	19.5	0.38	3	-9.4	0.08	3	158.3	21.0	1047	184.9	0.78	3	-8.2

Nanoparticle ID	C														
Time	0 hour									72 hour					
Type of DLS Characterization	Size by Peak[b]		Size by Z-Average[c]				Zeta Potential			Size by Peak		Size by Z-Average				Zeta Potential
	Mean (nm)	SEM	Mean (nm)	SEM	Mean PdI[f]	N	Mean (mV)	SEM	N	Mean (nm)	SEM	Mean (nm)	SEM	Mean PdI	N	Mean (mV)
Media with 10% FBS	44.3	3.1	35.2	3.4	0.44	3	-1.3	0.38	3	157.3	2.0	125.4	4.2	0.44	3	-6.9
0.3 µg/ml	231.6	23.7	495.6	38.7	0.51	3	-8.5	0.28	3	221.8	5.7	271.4	18.9	0.30	3	-9.2
3 µg/ml	289.7	18.5	367.4	24.6	0.39	3	-8.4	0.40	3	240.4	25.8	293.1	35.2	0.41	3	-9.8
30 µg/ml	331.2	7.4	437.2	12.5	0.42	3	-8	0.20	3	253.8	10.6	354.5	11.7	0.40	3	-9.2

Nanoparticle ID	D														
Time	0 hour									72 hour					
Type of DLS Characterization	Size by Peak		Size by Z-Average				Zeta Potential			Size by Peak		Size by Z-Average				Zeta Potential
	Mean (nm)	SEM	Mean (nm)	SEM	Mean PdI	N	Mean (mV)	SEM	N	Mean (nm)	SEM	Mean (nm)	SEM	Mean PdI	N	Mean (mV)
Media with 10% FBS	44.3	3.1	35.2	3.4	0.44	3	-1.3	0.38	3	157.3	2.0	125.4	4.2	0.44	3	-6.9
0.3 µg/ml	107.5	5.5	505.5	33.8	0.61	3	-9.2	0.23	3	160.1	25.7	415.3	84.0	0.40	3	-9
3 µg/ml	192	5.5	506.8	21.8	0.53	3	-5.3	0.80	3	261.4	32.9	309.8	44.1	0.46	3	-8.7
30 µg/ml	328	7.3	442.8	14.3	0.45	3	-8.9	0.32	3	300.9	11.4	332.6	2.0	0.37	3	-10.4

Nanoparticle ID	H														
Time	0 hour									72 hour					
Type of DLS Characterization	Size by Peak		Size by Z-Average				Zeta Potential			Size by Peak		Size by Z-Average				Zeta Potential
	Mean (nm)	SEM	Mean (nm)	SEM	Mean PdI	N	Mean (mV)	SEM	N	Mean (nm)	SEM	Mean (nm)	SEM	Mean PdI	N	Mean (mV)
Media with 10% FBS	13.9	3.5	48.4	22.1	0.12	3	ND			114.6	0.9	65.0	5.9	0.21	3	-8.1
0.3 µg/ml	154.3	3.6	795.9	58.0	0.75	3	-10.7	0.76	3	153.7	13.1	672.0	71.3	0.57	3	-10
3 µg/ml	321.7	18.3	599.8	33.6	0.45	3	-10.2	0.56	3	227.8	7.0	532.4	197.3	0.66	3	-8.9
30 µg/ml	452.7	8.7	572.2	8.2	0.34	3	-9.9	0.56	3	379.0	15.1	465.2	68.6	0.55	3	-9.5

Nanoparticle ID	I														
Time	0 hour									72 hour					
Type of DLS Characterization	Size by Peak		Size by Z-Average				Zeta Potential			Size by Peak		Size by Z-Average				Zeta Potential
	Mean (nm)	SEM	Mean (nm)	SEM	Mean PdI	N	Mean (mV)	SEM	N	Mean (nm)	SEM	Mean (nm)	SEM	Mean PdI	N	Mean (mV)
Media with 10% FBS	13.9	3.5	48.4	22.1	0.12	3	ND			114.6	0.9	65.0	5.9	0.21	3	-8.1
0.3 µg/ml	179.2	7.8	731.4	27.6	0.58	3	-5.8	0.37	3	159.1	13.7	584.4	66.0	0.51	3	-7.6
3 µg/ml	238	8.1	582.1	17.6	0.53	3	-8.7	0.44	3	259.2	19.3	337.1	77.3	0.41	3	-9.5
30 µg/ml	467.9	10.6	453.9	3.2	0.23	3	-9.4	1.07	3	234	13.8	348.7	21.6	0.33	3	-9.1

[a]Final measurement after 72 hours of incubation at 37°C.

[b]The predominant peak based on intensity analysis is reported.

[c]The Z-Average is the cumulants mean, expressing the mean hydrodynamic particle diameter.

[d]Standard error of the mean.

[e]Polydispersity index (PdI), a unitless measure of the width of the size distribution of the particles, ranging from 0 to 1.

Nano Particle	Low (0.3 μg/ml)	Mid (3 μg/ml)	High (30 μg/ml)	Sum of DEGs
A	6	420	610	1,036
B	190	664	1089	1,943
C	10	25	228	263
D	67	104	168	339
H	397	158	241	796
I	323	480	479	1,282

Table 2: number of differentially expressed genes (DEGs).

	A high	B high	C high	D high	H high	H low	I high
Particle size	31	59	25	22	214	214	142
surface area	52.9	22.2	118	49.8	11.6	11.6	6.99
crystal structure	A[a]> R[b]	A> R	A	A> R	R	R	A
agg. size at time 0	402.8	534.0	331.2	328.0	379.0	153.7	467.9
DEG	610	1089	228	168	241	397	479
DEG/Agg. Size	1.51	2.04	0.69	0.51	0.64	2.58	1.02
DEG/Surface area	11.53	49.05	1.93	3.37	20.78	34.22	68.53
# of pathway	11	60	13	22	29	41	51
1	EIF2 signaling	EIF2 signaling	Fatty acid activation	Glucocorticoid receptor signaling	EIF2 signaling	EIF2 signaling	EIF2 signaling
2	Caveolar-mediated endocytosis	Regulation of eIF4 and P70S6K signaling	gamma-linolenate biosynthesis II	Fatty acid activation	remodeling of epithelial adherens	Oncostatin M signaling	Cell cycle G2/M DNA damage checkpoint
3	Glycolysis	Integrin signaling	Mitochondrial L-carnitine shuttle pathway	gamma-linolenate biosynthesis II	14-3-3-mediated signaling	PI3K/AKT signaling	Mitotic roles of Polo-like kinase
4	Gluconeogensis	ERK5 signaling	CDK 5 signaling	Mitochondrial L-carnitine shuttle pathway	glucocorticoid receptor signaling	PDGF signaling	remodeling of epithelial adherens junctions
5	mTOR signaiing	Estrogen receptor signaling	Spermidine biosynthesis	ERK5 signaling	Acute phase response signaling	Acute phase response signaling	Regulation of eIF4 and p70S6k signaling
6	FAK signaling	VEGF signaling	Actin nucleation by ARP-WASP complex	Estrogen-dependent breast cancer signaling	Aryl hydrocarbon receptor signaling	Stearate biosynthesis	mTOR signaling
7	Glycogen degradation III	Acute phase response signaling	Spermidine biosynthesis	Hepatic fibrosis/hepatic stellate cell activation	Epithelial adherens junction signaling	Erb2-Erb3 signaling	ERK5 signaling
8	Regulation of eIF4 and p70S6K signaling	Protein ubiquitination pathway	5'-adenosyl-L-methionine biosynthesis	Fatty acid beta-oxidaation I	Gap junction signaling	DHA signaling	Integrin signaling
9	Fatty acid beta-oxidation	Actin nucleation by ARP-WASP complex	Tyrosine biosynthesis IV	Aldosteron signaling in epithelial cells	Oxidative ethanol degradation III	IGF-1 signaling	14-3-3-mediated signaling
10	Bile acid biosynthsis	LXR/RXR activation	Fatty acid beta-oxidation I	Stearate biosynthesis	Ethanol degradation IV	Regulation of eIF4 and P70S6K signaling	Stearate biosynthesis
11	NRF2-mediated oxidative stress response	FXR/RXR activation	Retinoate biosynthesis II	Protein ubiquintination pathway	Breast cancer regulation by Stathmin 1	ILK signaling	Coagulation system
12		Paxilin signaling	Phenylalanine degradation I	Spermine and spermindine degradation I	Regulation of eIF4 and p70S6k signaling	Glucocorticoid receptor signaling	Role of tissue factor in cancer
13		mTOR signaling	Atherosclerosis signaling	Proline biosynthesis I	Proline degradation	Fatty acid beta-oxidation I	Acute phase response signaling
14		Role of tissue factor in cancer		melatonin degradation II	Uridine-5'-phosphate biosynthesis	Glycogen degradation III	Sucrose degradation V
15		Tetrahydrobiopterin biosynthesis I		Cell cycle: G2/M DNA damage checkpoint regulation	4-hydroxylproline degradation I	PTEN signaling	Glycolysis I

Table 3: Top canonical pathways from IPA

protein metabolism related pathways

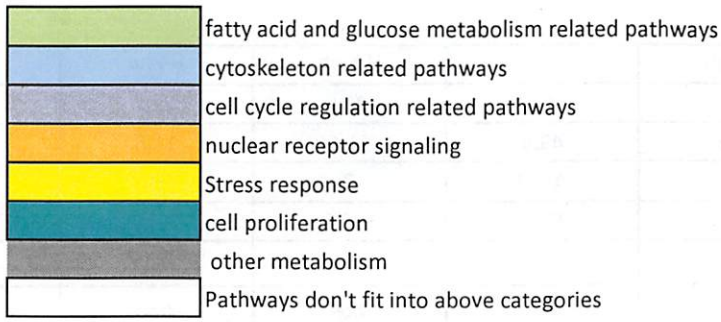

a:
Anatase

b:
Rutile

functional categories	canonical pathways	A high	B high	C high	D high	H high	H low	I high	
crystal structure		A[a]> R[b]	A> R	A	A> R	R	R	A	
surface area		52.9	22.2	118	49.8	11.6	11.6	6.99	
Primary Particle size		31	59	25	22	214	214	142	
Agg. size at high dose		402.8	534.0	331.2	328.0	452.7	154.3	467.9	
DEG		610	1089	228	168	241	397	479	
Stress Response	Mitochondrial dysfunction	----	----	---	----	----	30	----	1
	Acute Phase Response Signaling	----	**7**	---	----	**5**	**5**	**13**	**4**
	NRF2-mediated Stress Response	11	40	----	----	----	----	----	2
	Hepatic fibrosis/hepatic stellate cell activation	----	----	----	7	----	----	----	1
Protein Synthesis/ degradation	EIF2 signaling	**1**	**1**	----	----	**1**	**1**	**1**	**5**
	mTOR singaling	**5**	**13**	----	----	**26**	**39**	**6**	**5**
	Regulation of eIF4 and P70S6K signaling	**8**	**2**	----	----	**12**	**10**	**5**	**5**
	Protein Ubiquitination pathway	----	8	----	11	----	----	18	**3**
Cell cycle/cell proliferation	Cell Cycle: G2/M DNA damage Checkpoint Regulation	----	28	----	15	----	----	2	**3**
	Myc-mediated apoptosis	----	33	----	----	----	----	----	1
metabolism	Fatty Acid Activation	----	----	**1**	**2**	----	**20**	**31**	**4**
	Mitochondrial L-carnitine Shuttle Pathway	----	----	**3**	**4**	----	**34**	**50**	**4**
	Fatty acid beta oxidation	----	----	10	8	----	13	----	3
	Glycolysis	3	----	----	----	----	----	15	2
	Cholesterol biosynthesis		37, 38,						1
	FXR/RXR signaling		11						1
Cancer related pathways	Role of tissue factor in cancer		14					12	2
	Breast cancer regulation by Stathmin 1					11			1
	Non-small cell lung cancer signaling						26		1
	Glioma invasiveness signaling		30						1
	Estrogen-dependent breast cancer signaling				6				1
Inflammation	complement		29			25			2
Endocytosis	Caveolar-mediated endocytosis Signaling	2	31	----	----	----	----	----	2
	clathrin-mediated Endocytosis Signaling	----	17	----	----	27	----	17	3
	Macropinocytosis	----	53	----	----	----	----	----	1

a: Anatase

b: Rutile

Table 4. Ranking of selected canonical pathways from Ingenuity Pathway Analysis. --- means not present on the list ($p \leq 0.05$); Pathways affected by 4 or more treatments are highlighted and the numbers are bolded.

	A	B	C	D	H	I
surface area	52.9	22.2	118	49.8	11.6	6.99
dry particle size	31	59	25	22	214	142
agglomerated size (30 µg/ml)	402.8	534.0	331.2	328.0	452.7	467.9
crystal structure	anatase > rutile	anatase > rutile	anatase	anatase > rutile	rutile	anatase
immuno-spin trapping[a] (30 ug /ml)	NE	NE	NE	NE	NE	NE
immuno-spin trapping[a] (100 ug /ml)	medium increase	NE	large increase	small increase	small increase	NE
GSH (reduced)	**80%**	**87%**	**66%**	**NOT DONE**	**NOT DONE**	NO
decreased free fatty acids	**NO**	**Yes**	**NO**	**NOT DONE**	**NOT DONE**	**Yes**
change in a.a and peptides levels	**Yes**	**Yes**	**Yes**	**NOT DONE**	**NOT DONE**	**Yes**
change in metabolites in glycolysis and gluconeogenesis	**Yes**	**Yes**	**Yes**	**NOT DONE**	**NOT DONE**	**Yes**
fatty acid activation/L-carnitine shuttle pathway	NO	NO	YES	YES	Yes, in low dose	Yes
protein synthesis	YES	YES	NO	NO	YES	YES
Glycolysis	YES	NO	NO	NO	NO	YES
NRF2-mediated stress response	YES	YES	NO	NO	NO	NO
Acute phase response signaling	NO	NO	NO	NO	YES	YES
Mitochondrial dysfunction	NO	NO	NO	NO	NO	YES, in low dose
apoptosis	NO	yes	NO	NO	NO	NO
Cell cycle regulation	NO	YES	NO	YES	NO	YES
hepatic fibrosis	NO	NO	NO	YES	NO	NO
Cancer sigaling	NO	YES	NO	YES	YES	YES

Table 5. Summary table of 6 nano-TiO2 effects

	data from genomic study
	data from metabolomic study

a : Kitchin et al., 2011

NE No Effect

ID	Chemical	Vendor	Cat No.	Lot Number	Primary Particle Size (nm)	Size Range (nm)	Surface Area (m2/gr)	% Purity	Crystal Form	Assayer
A	TiO2	Degussa	AEROXIDE® P25	4165012298	27.5	14-64	49	95.1	86% anatase, 14% rutile	Vendor
					31	12-88	52.9	99.9	anatase and rutile	Univ Kentucky
B	TiO2	NanoAmor	5485HT	5485-030007	30-40	30-40	>30	95.1	rutile	Vendor
					59	36-97	22.22	99.9	anatase > rutile	Univ Kentucky
C	TiO2	Alfa Aesar	44690	D22T034	10		100-130		anatase	Vendor
					25	6-60	118	98.8	anatase	Univ Kentucky
D	TiO2	Alfa Aesar	39953	C27R043	32		45	99.9	anatase	Vendor
					22	9-61	49.8	97.7	anatase > rutile	Univ Kentucky
H	TiO2	MknaNo	MKN-TiO2-R250	495/2007	200-400		6.8	99.97	rutile	Vendor
					214	37-410	11.6	98.7	rutile	Univ Kentucky
I	TiO2	Acros	21358	A0075656	Ave. 200				anatase	Vendor
					142	67-322	6.99	99.9	anatase	Univ Kentucky

Supplemental Table 1. Physical-chemical properties of nano-TiO_2

supplemental table 2

		A	B	C	D	H	H low	I	I mid
primary particle size (nm)		31	59	25	22	214		142	
crystal structure		A> R	A> R	A> R	A> R	R	R	A	A
a. Metabolomics analysis		YES	YES	YES	ND	ND	ND	YES	YES
GSH		-5	-7.7	-2.9	ND	ND	ND	NC	NC
long chain fatty acid		NC	NC	NC	ND	ND	ND	down (some)	down (more)
lysolipids		NC	NC	NC	ND	ND	ND	down	NC
sphingolipids		up	NC	up	ND	ND	ND	NC	NC
b. Mitochondrial dysfunction							**Sig. altered**		
over all change		NC	I, III, V	I up	NC	II up	III, IV, and V up	III, V down	
	Complex I								
genomics	NDUFAF2		1.6[a]						
	NDUFB3		1.8						
	NDUFB7		-1.56						
	NDUFS8		-1.57						
	NDUFS7		-1.56	1.50					
	complex II								
genomics	SDHC					1.8			
	SDHD					1.7			
	complex III								
genomics	UQCRB		2				1.55	-1.70	
	UQCRH		1.55						
	Complex IV								

genomics	COX7B						1.98		
	complex V								
genomics	ATP5D		-1.9						
	ATP5E						1.54		
	ATP5F1		2.2						
	ATP5G1							-1.53	
total number of altered genes in complex I to V			9	1	0	2	3	2	
Other genes/proteins in mitochondria									
genomics	APP (Amyloid b, C161)				-2.06	2.10	-1.84	1.82	
	PRX3	1.54	2.2						
	Furin		-1.6				-1.50		
metabolomics	NAD+	-1.49		-1.3					
	GSH	-5	-7.7	-2.9					
	citrate		-1.49					-1.28	

c. NRF2 signaling		sig. Altered	sig. Altered						
NRF2				-1.6					
RAS			1.7						
PI3K			ATM: 1.6						
AKT			-1.6						
MEK1/2 = MAP2k2			-2.1			1.7	-1.7		2
GPX			-1.6			1.8			
MAFG		1.7	-1.5			1.5			
TXN			1.6						
EPHX1, epoxide hydrolase 1			-1.6						
Actin		up/d	2.2				2.5	-1.7	
SR-B1			d						
STIP1		1.8	-1.6		-1.54	1.8		1.5	1.5
TXNRD1		2					-1.5		
HSP22/40/90		HSP90: 1.5	HSP90AA1: 1.8	HSPB1: 1.6			DNAJB6: 1.6		
AOX		1.5							
CCT7		-1.7	1.8				2.2	-1.8	-1.8
GST								MGST1:-1.8	MGST!: -2.0
GCLM								-1.5	
ERP29								-1.7	
PTPLAD1						1.6			

d. Acute phase response			sig. altered			sig. altered	sig. altered	sig. altered	
IL1RN		-1.9	1.8			-1.5	2	-1.6	
TNFR			-1.5						
GP130			1.7						
RAS			1.7						
AKT			-1.7						
MEK1/2			-2.1			1.7	-1.7		
TCF 3/4			-1.6					1.7	
HNRPK		-4.3	2.8						
C3			-1.9			2.5	1.8		
A2M			-1.8					1.9	
HAMP			-1.8				-1.6		
C4BP		-1.5	1.6						
SERPIND1			-1.5						
SERPINF			-1.9					1.8	
C2			-2			1.6			
SERPING1			-1.6						
APOH		-1.5							
RBP		1.9		1.6		-1.7	-1.7	-1.5	
FGB								1.9	
FGG								1.6	
C5								1.5	
HP						1.6	1.5	1.5	
SERPINE1				-1.4	-1.8	1.5			
SHC1							-1.5		
OSMR							1.8		

e. Hepatic fibrosis					**Sig. altered**				
Leptin (fibrogenic)					1.5				
Il-10 (antifibrotic)					1.8				
IGFBP4 (fibrogenic)			-1.79		-1.7				
PAI-1 (SERPINE1, plasminogen activator inhibitor 1)) (fibrogenic) usually induced in liver fibrosis					-1.8				

f. cell cycle			Sig. altered		Sig. altered			Sig. altered	
CCND		1.5					-1.6		
G2/M			Arrest??		slowed			slowed	
14-3-3		YWHA E:1.5	YWHA b, e, z: 1.7, 2.0, 1.6				YWHA e: 1.6	YWHA b, e: -1.6, -1.5	
ATM			**1.63**						
CCNB					-1.5			-1.6	
Cdc2 (CDK1)			1.7					-1.9	
Cdc25b/c							-1.6		
CKS1								-1.8	
CKS2		-1.7	1.5					-1.6	
p21 CIP						-1.5			
PIK1(positive regulator for G2/M)								-1.5	
Topo II					-1.8				

EIF2		**Sig. altered**	**Sig. altered**			**Sig. altered**	**Sig. altered**	**Sig. altered**	
overall change		down	?	NC	NC	?	?	down	
PI3K		NC	ATM: 1.6	NC	NC	NC	NC	NC	
RAS		NC	1.7	NC	NC	NC	NC	NC	
AKT		NC	-1.7	NC	NC	NC		NC	
MEK1/2		NC	-2.1	NC	NC	1.7	-1.7	NC	
EIF3		mostly down	mostly up	NC	NC	NC	2.3	mostly down	
EIF4		mostly down	mostly up	NC	NC	mostly up	mixed	mostly down	
PDK1		-1.9	NC	NC	NC	NC	1.7	NC	
40 S ribosomal subunit		mostly down	mixed,	NC	NC	mostly down	all up: 9 genes	mostly down	
60 S ribosomal subunit		mostly down	mixed: mostly up	all up: 4 genes	all up: 3 genes	all down	all up: 20 genes	mostly down	
SHC							-1.5		

NC: No change; NE: Not Done

Supplemental Table 2. Gene list and expression levels of pathway genes for 5 major areas (metabolomics analysis, mitochondrial dysfunction, NRF2 signaling, acute phase response, hepatic fibrosis and cell cycle).

[a]: Fold change for parameter

Supplemental Information:

Physical-chemical characterization information for nano TiO_2 D and H.

Sample D.

This table lists the data supplied by the EPA as provided by the manufacturer or source.

Sample ID	D
Vendor	Alfa Aesar
Composition	TiO_2
Catalogue number	39953
Primary particle size, nm	32
Size range, nm	-
Surface area, m^2/g	45
% purity	99.9
Crystal form	anatase
Lot number	C27R043

1. Elemental analysis by TEM/EDX

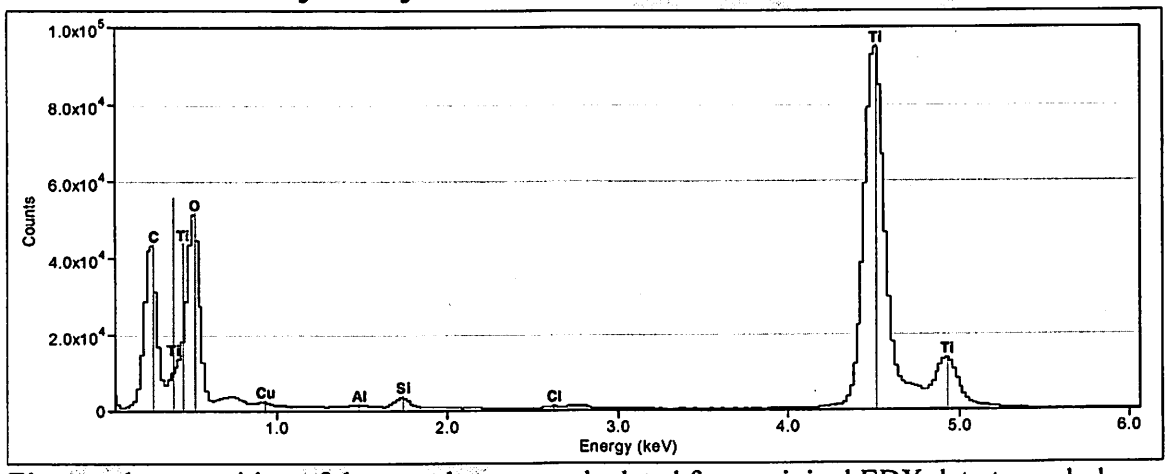

Elemental composition of the sample was recalculated from original EDX data to exclude Si, which was found in the sample background. Although it is possible that Si is present in the sample, it could not be distinguished from the background Si.

Quantification Results
Correction method: Thickness

Element	Weight %	Atomic %	Detector Uncertainty %	Absorption Correction	k-Factor	Correction
O(K)	32.369	58.333	0.068	0.514	1.980	1.000
Al(K)	0.694	0.742	0.009	0.965	1.040	1.000
Si(K)	1.493	1.532	0.011	0.977	1.000	1.000
Ti(K)	65.442	39.392	0.073	0.985	1.299	1.000

Si and Cl on this EDX spectrum are also present in the background, and cannot be confirmed by this analysis.

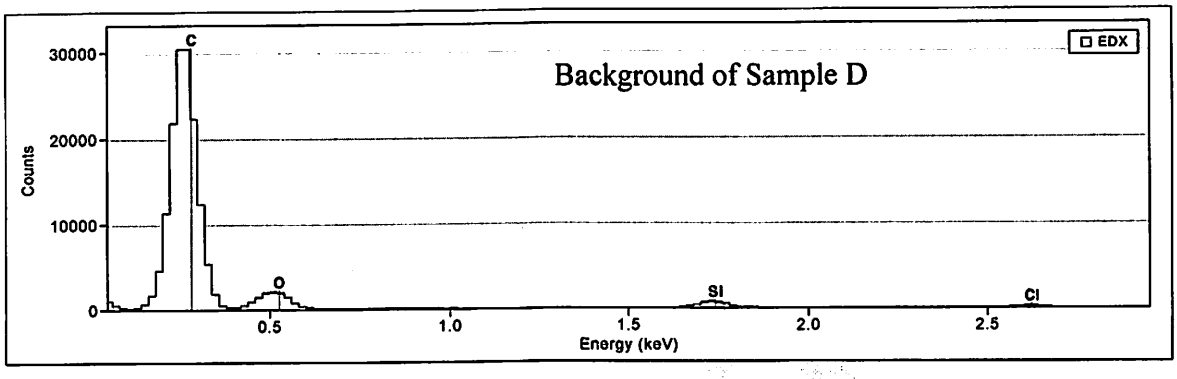

Quantification Results Background of Sample D
Correction method: Thickness

Element	Weight %	Atomic %	Detector Uncertainty %	Absorption Correction	k-Factor	Correction
C(K)	96.565	97.664	0.262	0.173	6.279	1.000
O(K)	2.670	2.027	0.024	0.514	1.980	1.000
Si(K)	0.509	0.220	0.007	0.977	1.000	1.000
Cl(K)	0.254	0.087	0.005	0.936	1.138	1.000

2. Elemental analysis by ICP

Ti = 59.95%
Certified SPEX TiO_2 standard; Ti = 59.93%.
Theoretical titanium level in TiO_2; Ti = 59.95%.
The contaminants with the highest concentrations in the SPEX TiO_2 standard were: Co (753 ppm), P (25 ppm), SiO2 (538 ppm), and V (250 ppm).

Because the sample showed high purity, the ICP/MS system was set up to find contaminants, rather than directly measure the titania concentration. A set of thirty-one elements was checked, as shown in the master table for this analysis. The levels of contaminants in the highest concentration were: Co (608 ppm), Fe (131 ppm), SiO_2 (495 ppm) and V (171 ppm).

3. Specific surface area/porosity by BET

The BET surface area is 49.8 m^2/g. If the sample were individual primary particles that were not aggregated, the average diameter would be 31 nm. The TEM photomicrographs suggests an average primary particle size of 19 nm, which would correspond to a surface area of ~82.2 m^2/g for discrete primary particles. As discussed in the next section, Sample D appears to have a multimodal particle size distribution, with a peak centered an

order of magnitude larger than the primary particle size measured by TEM. This type of distribution would result in a measured surface area lower than that estimated from the average diameter of the smallest peak.

Test/estimate	**Surface area, m^2/g**	**D_{av}, nm**
BET result, estimate of discrete primary particle size	**49.8**	31.4
D_{av} result, estimate of primary particle surface area	82.2	**19**

BET measurements of Sample D

Measurement	**PR-NC-08-10414**
BET, m^2/g	47.7
BJH adsorption cumulative surface area of pores, m^2/g	51.0 (0.85-150 nm)
BJH desorption cumulative surface area of pores, m^2/g	53.8 (0.85-150nm)
Single point surface area, m^2/g	47.7 (P/P_0=0.300)
BJH adsorption cumulative pore volume, cm^3/g	0.30
BJH desorption cumulative pore volume, cm^3/g	0.30
t-plot micropore area, m^2/g	0.85
t-plot external surface area, m^2/g	48.9
BJH adsorption pore diameter (4V/A), nm	11.6
BJH desorption pore diameter (4V/A), nm	10.9

4. Primary and aggregated size by TEM and DLS

TEM images show nearly spherical primary particles with a wide range in particle size distribution.

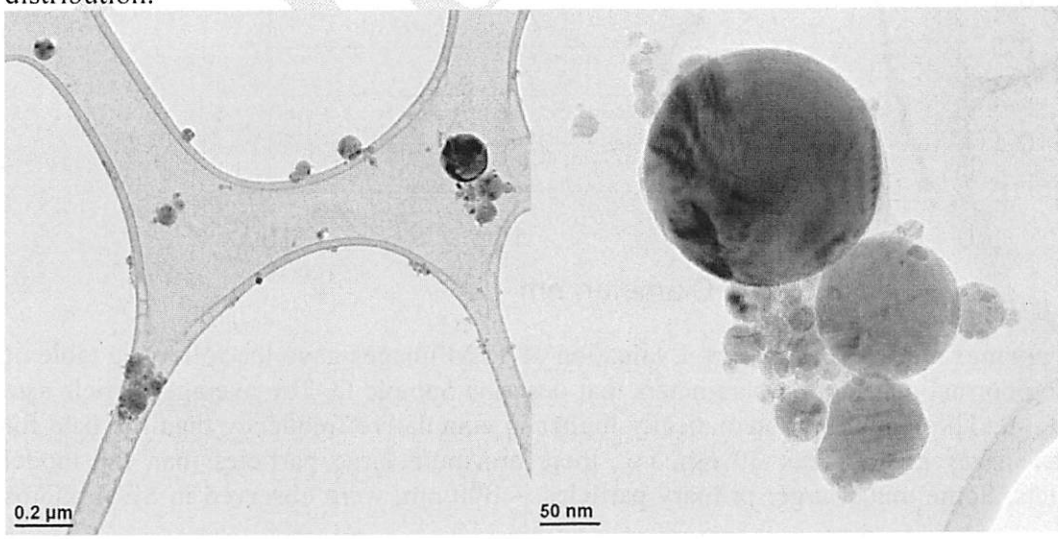

Figure 4.1 a&b. Sample D. Few large aggregates are visible (RHS), and the primary particles appear to be agglomerated rather than aggregated (LHS).

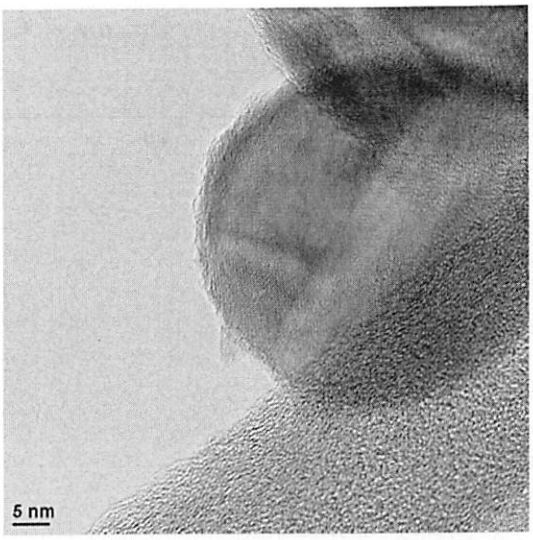

Figure 4.2. Sample D nanoparticles on the edge of the lacey carbon grid.

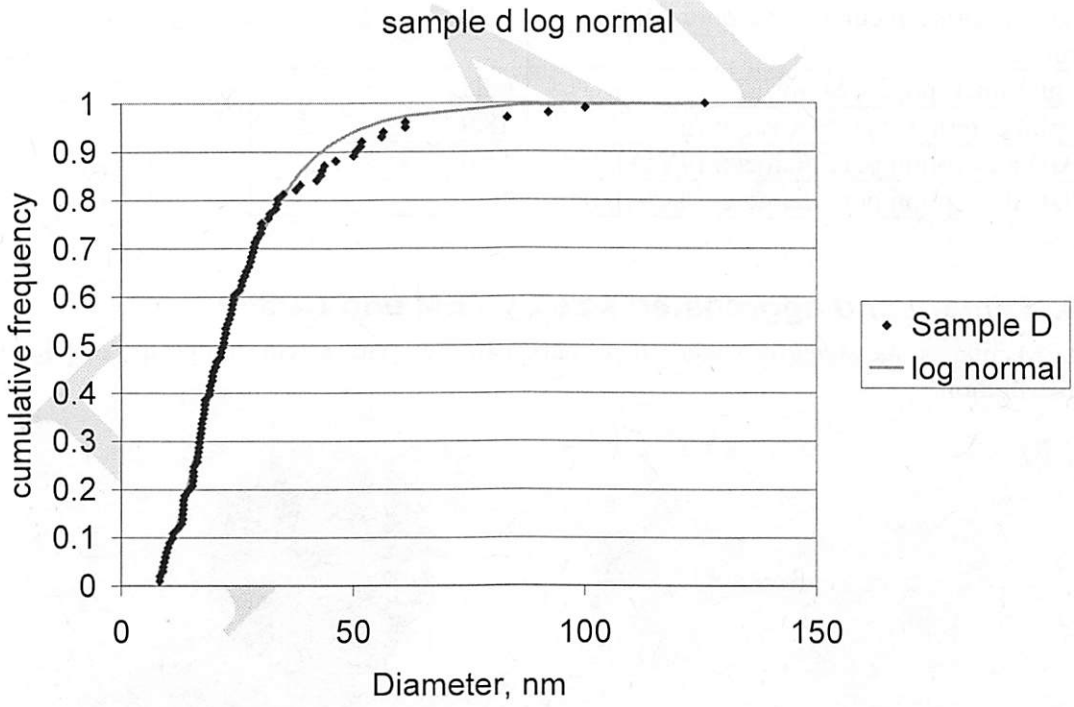

Log normal model parameters. Evaluation of TEM images gave the following table of the log normal distribution parameters that describe Sample D. The average particle size is 19 nm. The model is systematically higher in cumulative frequency than the data for particle sizes greater than 30 nm, i.e., there are more large particles than the model predicts. Some much larger primary particles, ~ 300 nm, were observed in SEM photos

but not in the TEM images. Sample D likely has a multimodal particle size distribution, with one peak centered near 20 nm, another near 100 nm, and a third near 300 nm.

Log normal model coefficients

Coefficient	Estimate	Average standard error	Estimate/A.S.E.
Mean, lnμ [exp(μ) = 19 nm]	2.931	0.005	831
Standard dev., σ	0.527	.006	83.6

Diameter range, 90% of sample fraction

	D_{05}, nm	Average diameter, nm	D_{95}, nm
Data	8	18	52
Model	8	18	44

5. Crystal structure by XRD

XRD pattern of the sample was matched with JCPDS cards # 21-1272 and #21-1276 which correspond to anatase and rutile. This sample contains mixture of anatase and rutile with anatase being predominant phase.

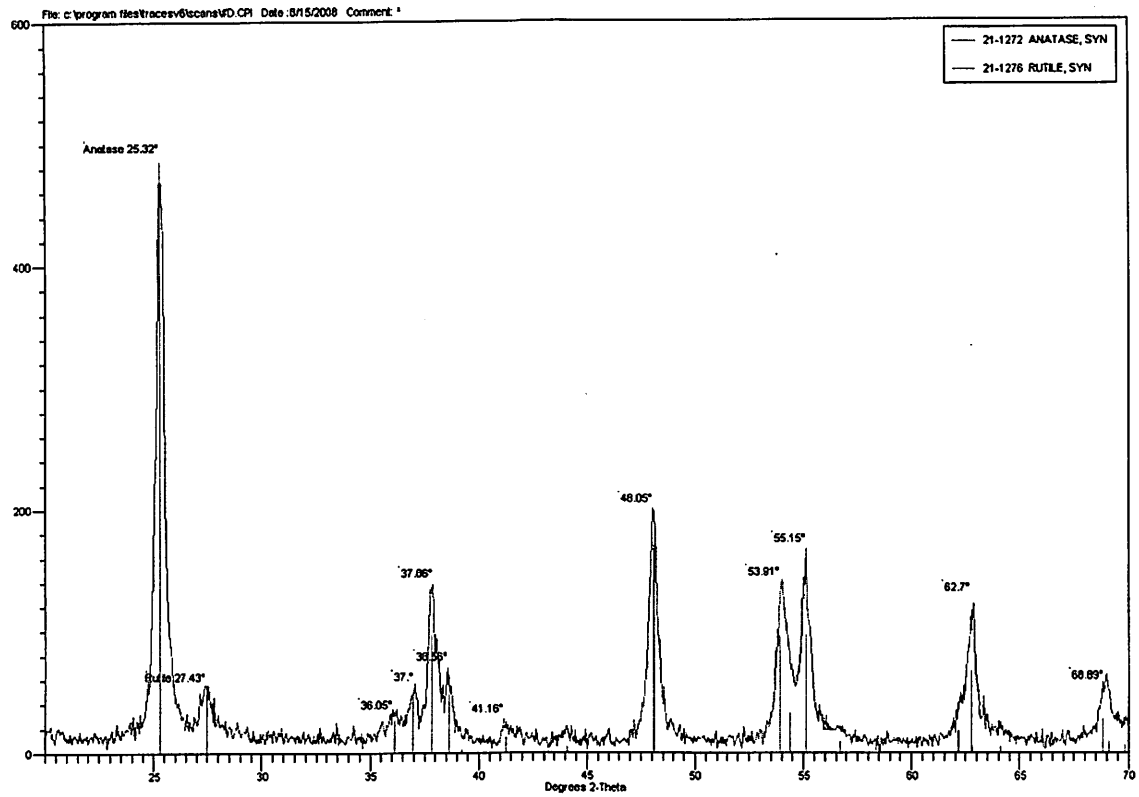

6. Elemental analysis

The elemental analysis results showed little carbon (< 0.05%), hydrogen (0.24%) and nitrogen (< 0.12%). These results are typical for high purity inorganic solids with sorbed water.

The elemental analysis of the SPEX titania standard was: carbon (< 0.05%), hydrogen (< 0.01%) and nitrogen (< 0.01%).

7. Particle shape and morphology by TEM and SEM

Nanoparticles in this sample are almost perfect spheres. They exhibit little aggregation, there is a wide particle size distribution, and they are crystalline. Two analyses reveal evidence of functionalization or contamination – TEM/EXD detects Al .

Table 7-1. Primary particle and aggregate sizes.

Method	Particle type	#	D_{av}, nm	Range, nm	Comments
TEM	Primary	101	22	9-61	Individual primary nanoparticles observed.

	agglomerates				No obvious fusion between primary particles.
DLS	1st peak	NA	100	92-129	
	2nd peak	NA	650	480-675	
SEM	Primary		~300		Observed in several images
	Aggregates		1-25 μm		Most of the mass is the largest aggregates

Sample ID	Sample D (Combined)
Operator ID	NM
Elapsed Time	00:05:00
Mean Diam.	228.1 nm
Rel. Var.	0.498
Skew	3.257

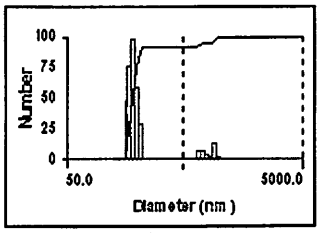

d(nm)	G(d)	C(d)	d(nm)	G(d)	C(d)	d(nm)	G(d)	C(d)
129.4	0	0	280.7	0	92	608.9	0	92
138.8	0	0	301.2	0	92	653.4	6	94
149.0	0	0	323.1	0	92	701.0	6	96
159.8	48	14	346.7	0	92	752.1	2	96
171.5	77	37	372.0	0	92	807.0	0	96
184.0	100	67	399.1	0	92	865.9	11	100
197.4	58	84	428.3	0	92	929.0	1	100
211.8	28	92	459.5	0	92	996.8	0	100
227.3	0	92	493.0	0	92	1069.5	0	100
243.8	0	92	529.0	0	92	1147.5	0	100
261.6	0	92	567.5	0	92	1231.2	0	100

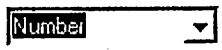

DLS.

The DLS sample was sonicated and the number frequency distribution is shown below. The smallest size fraction observed (100 nm) is larger than the maximum primary particle measured in TEM (60 nm); it appears likely that sonication did not completely fracture the aggregates to primary particles. The volume frequency plot shows a second aggregate peak near 650 nm in length scale.

SEM images with arrows pointing to large primary particles ~350 nm in diameter. The rest of the primary particles are much smaller.

PR-NC-08-10414. Sample D

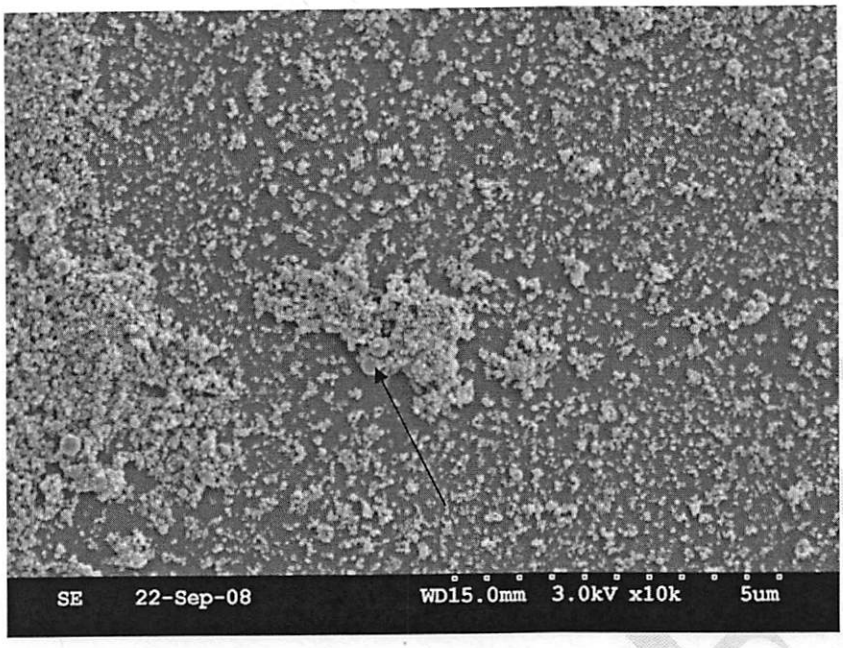

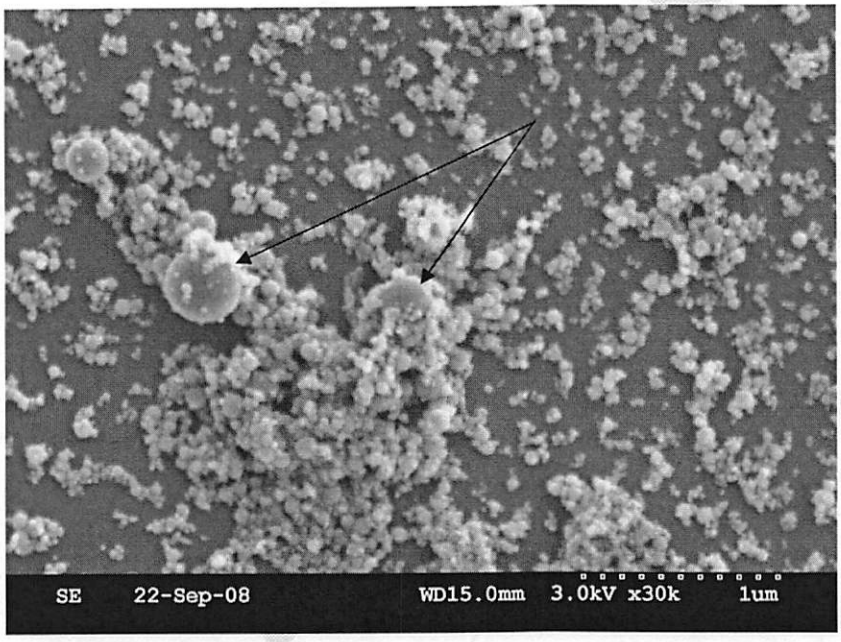

Appendix

D. Sample TiO_2, Alfa Aesar, Cat No. 39953, Lot No. C27R043

4. Primary and aggregated size by TEM and DLS

Primary size of the particles was determined by using Digital Micrograph program from Gatan (files in .dm3 format). Parameters of only clearly visible and non-overlapping particle could be determined by this method. Each random qualified particle was outlined manually and analyzed by the software.

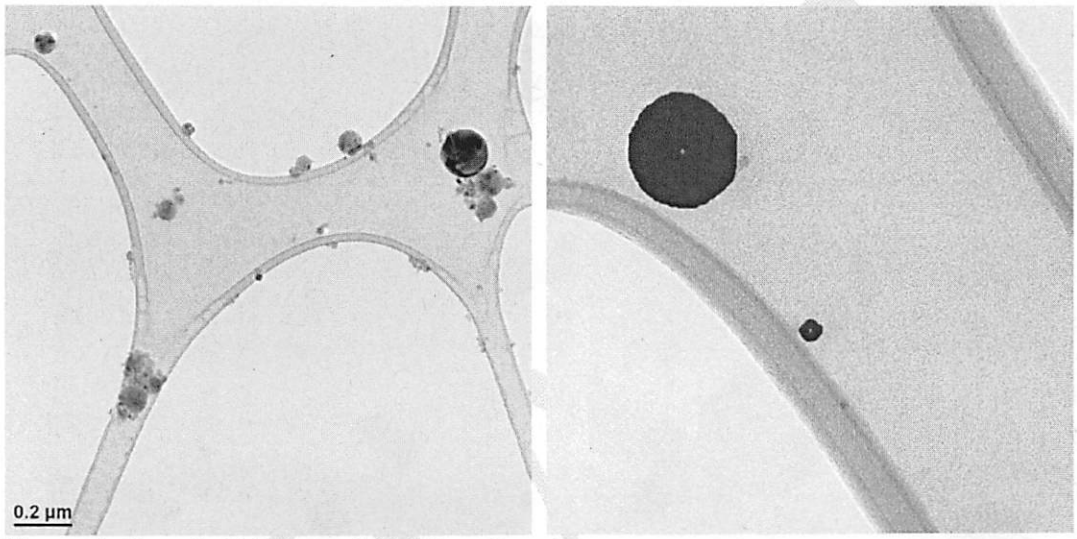

Figure 1. Sample D Images 1 and 2 analyzed

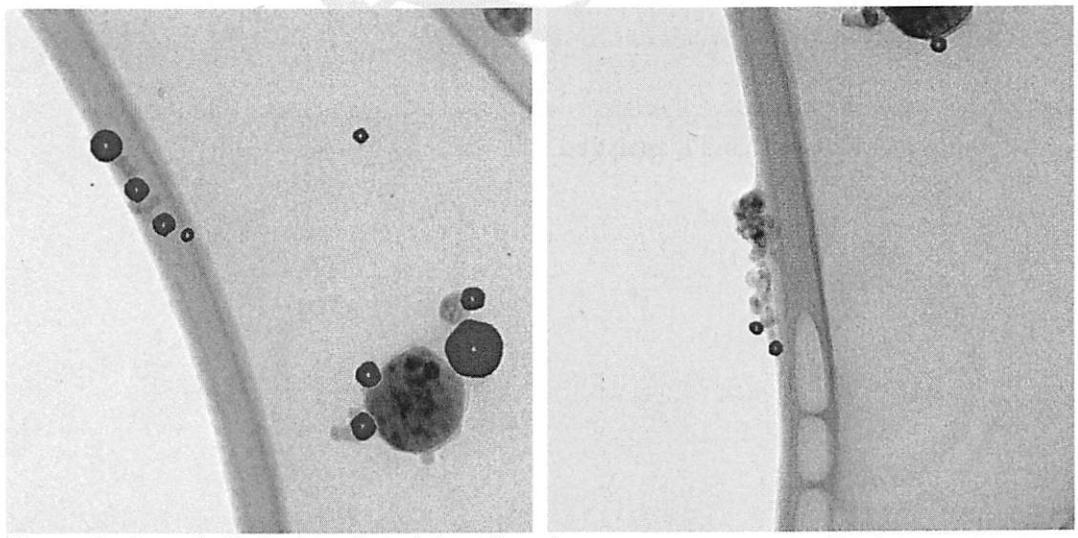

Figure 2. Sample D Images 3 and 4 analyzed

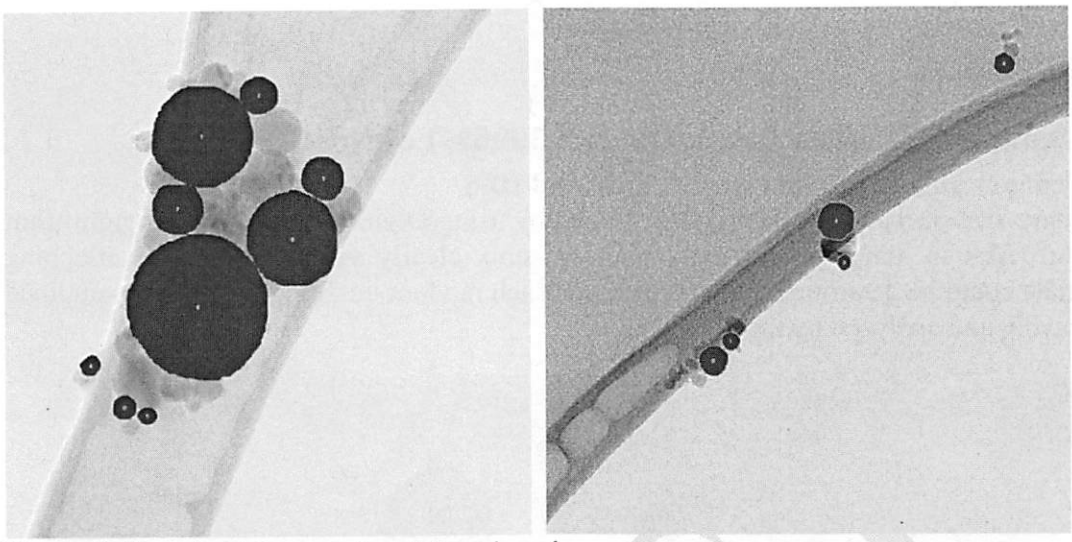

Figure 3. Sample D Images 5 and 6 analyzed

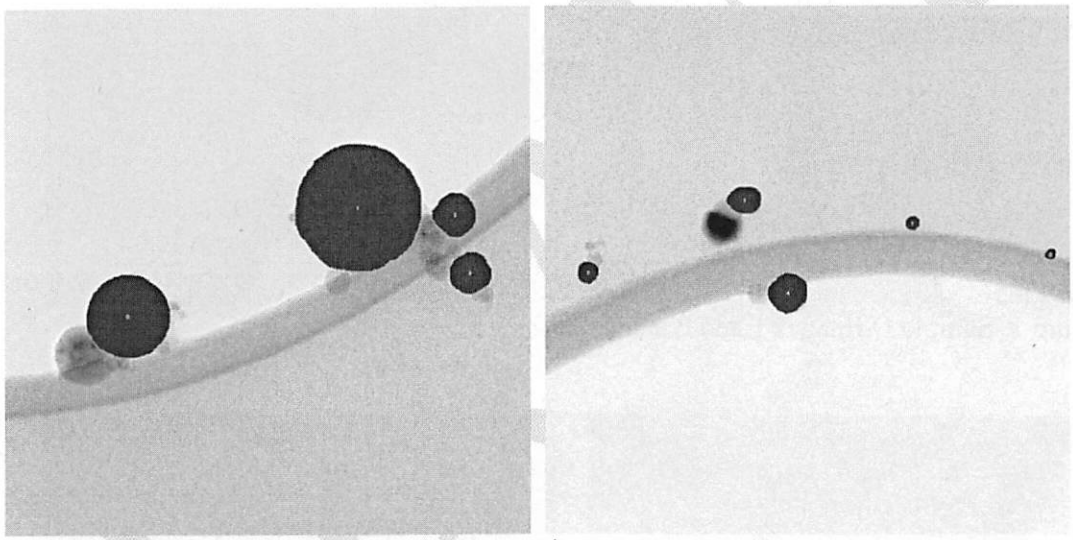

Figure 4. Sample D Images 7 and 8 analyzed

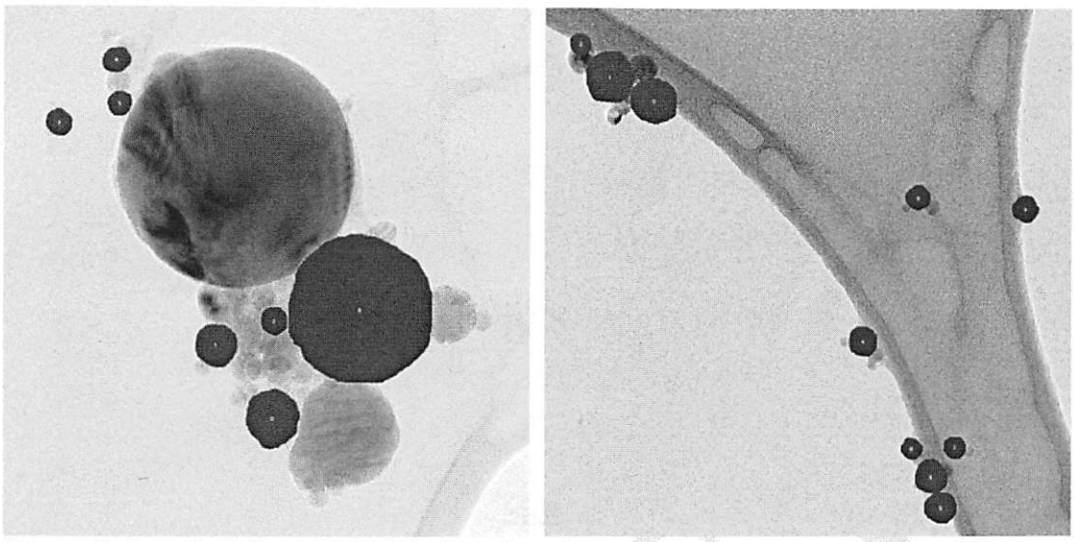

Figure 5. Sample D Images 9 and 10 analyzed

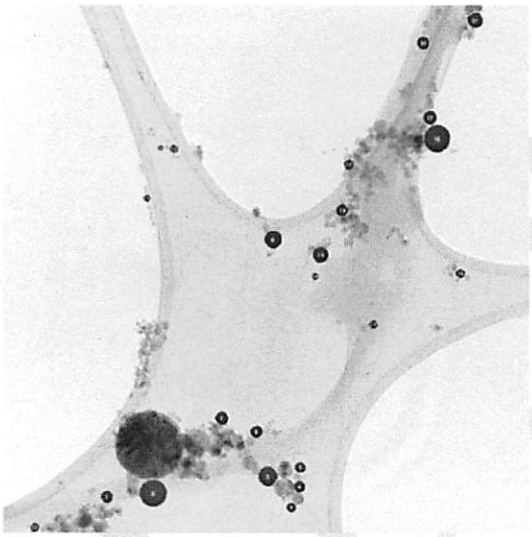

Figure 6. Sample D Image 12 analyzed

7. Particle shape and morphology by TEM and SEM

TEM images of the sample

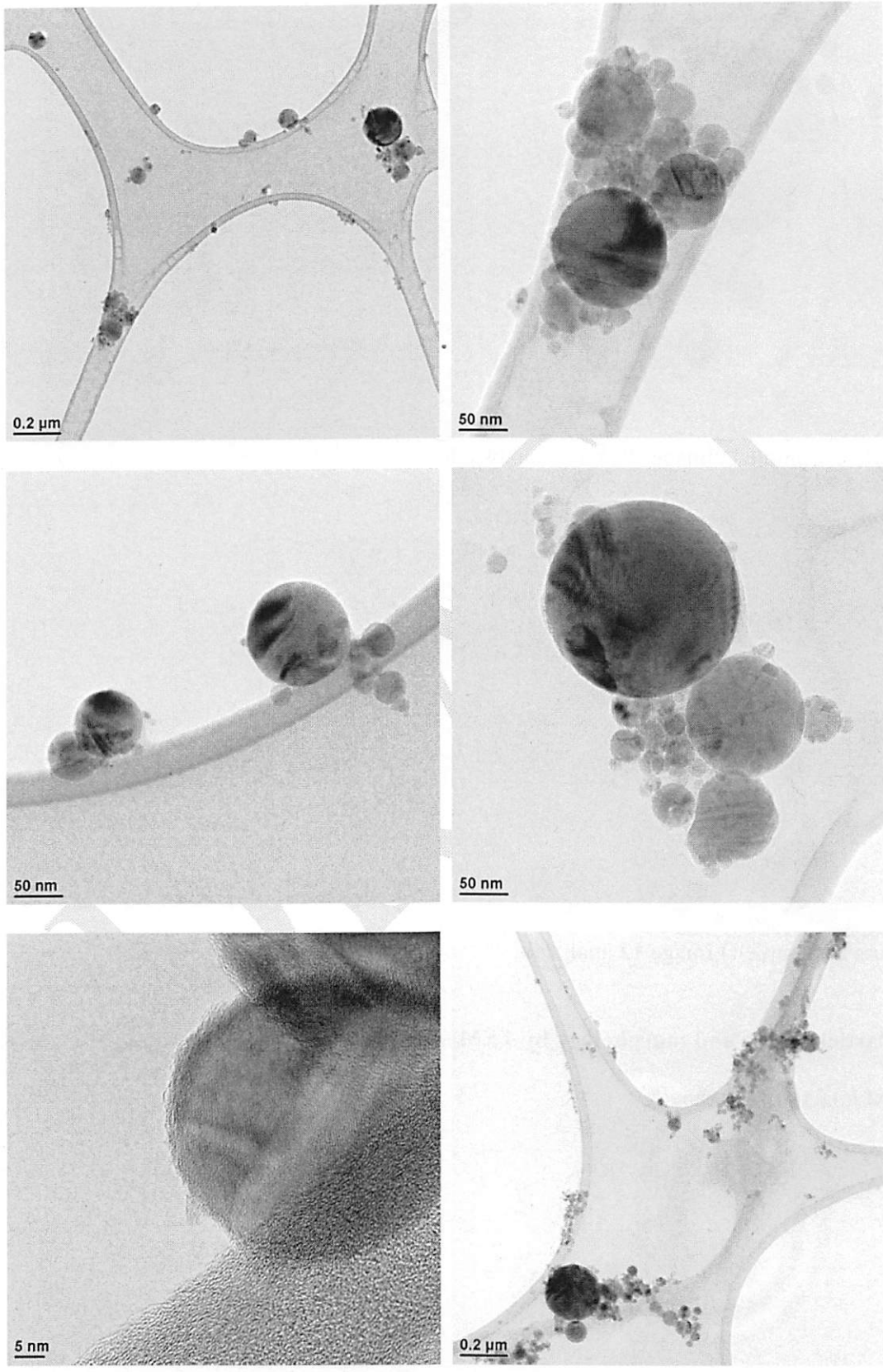
0.2 µm
50 nm
50 nm
50 nm
5 nm
0.2 µm

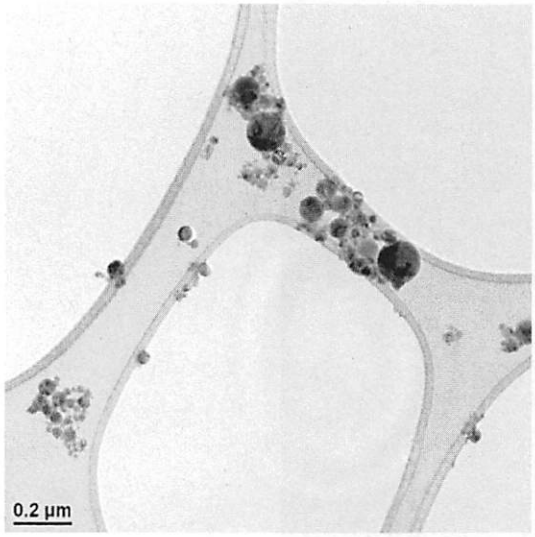

SEM images of the sample

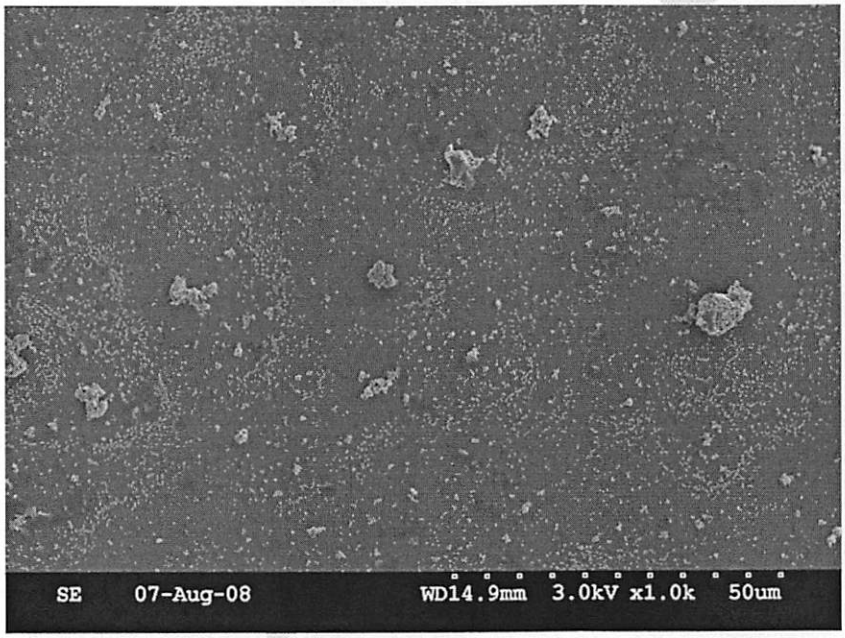

PR-NC-08-10414. Sample D

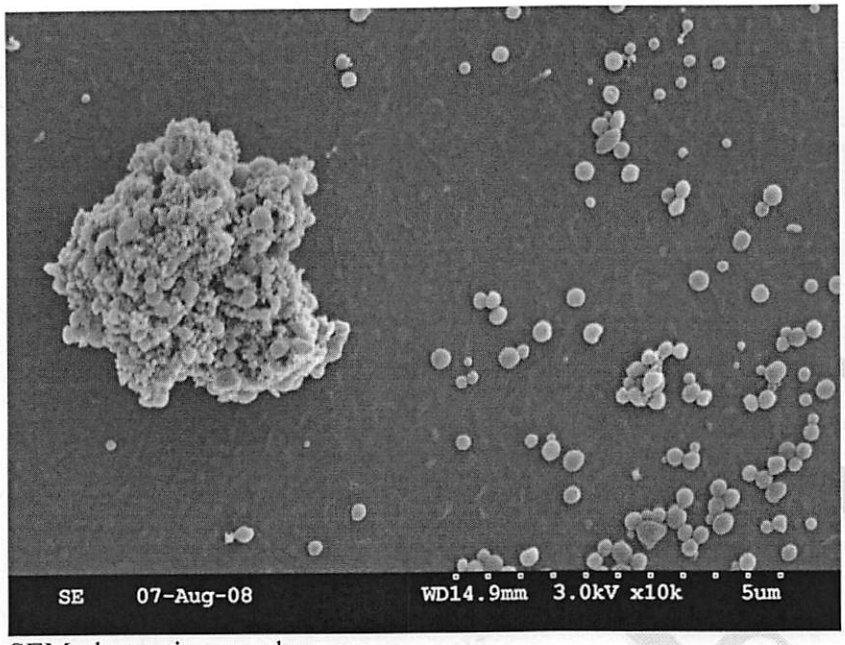

SEM photomicrographs

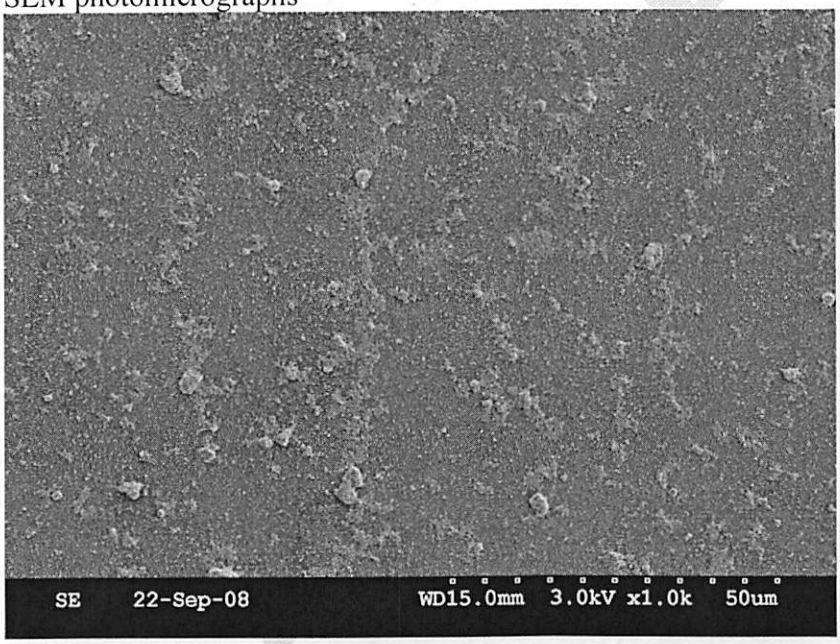

PR-NC-08-10414. Sample D

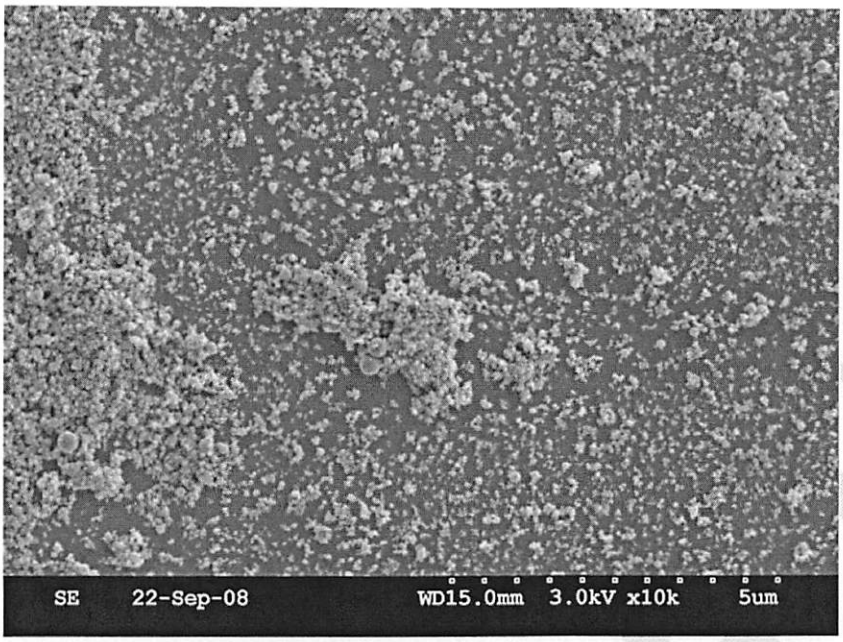

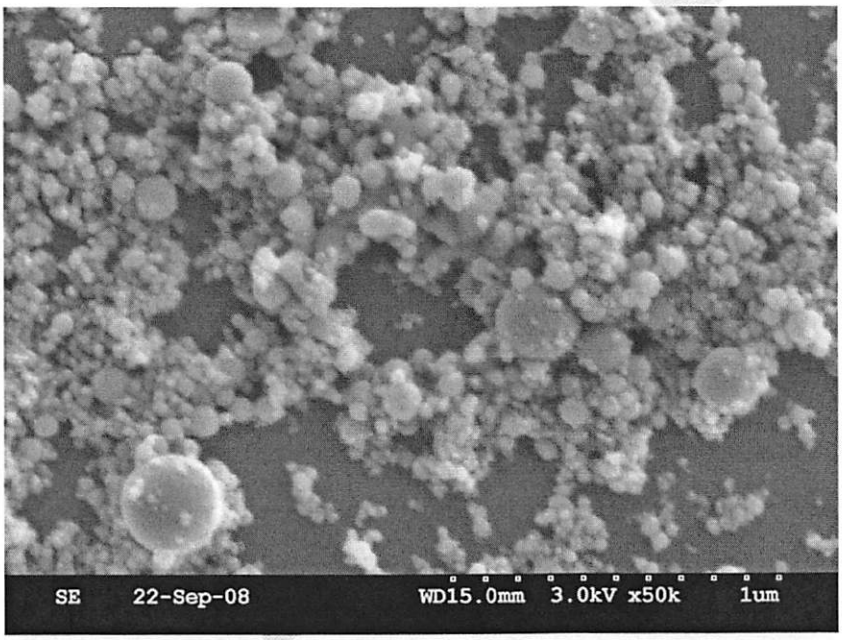

Sample H.

This table lists the data supplied by the EPA as provided by the manufacturer or source.

Sample ID	H
Vendor	Mknano
Composition	TiO_2
Catalogue number	MKN-TiO2-R250
Primary particle size, nm	200-400
Size range, nm	-
Surface area, m^2/g	6.8
% purity	99.86
Crystal form	rutile
Lot number	459/2007

1. Elemental analysis by TEM/EDX

Output of the EDX data depends on the several factors such as a position of the sample (above the Lacey carbon or on the side of Lacey carbon), position of the spot (in the middle of the sample or at the edge of the sample), and morphology of the particles.
Below are two examples that demonstrate difference of EDX results. In first example, the spot was positioned in the middle of the sample. In second example, the spot was positioned close to the edge of the sample.

Example 1. Spot was positioned in the middle of the sample

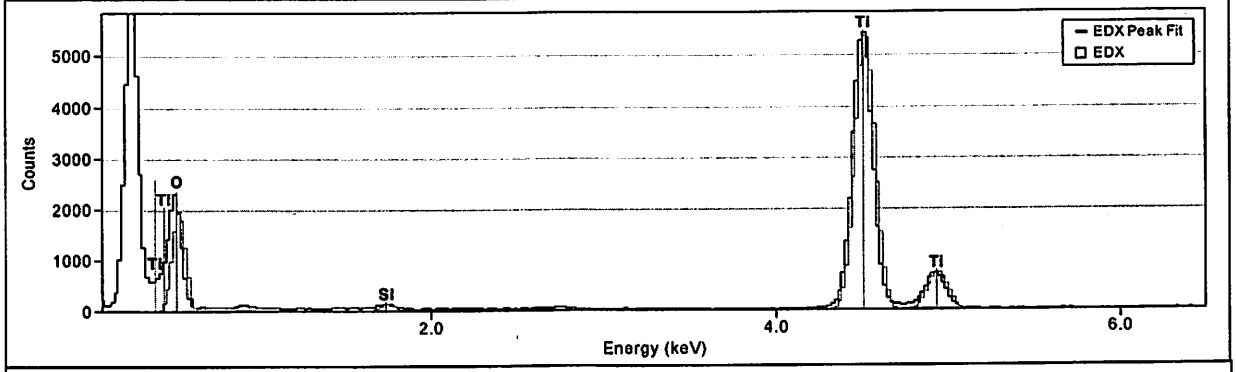

Quantification Results
Correction method: Thickness

Element	Weight %	Atomic %	Detector Uncertainty %	Absorption Correction	k-Factor	Correction
O(K)	26.417	51.508	0.295	0.514	1.980	1.000
Si(K)	1.243	1.380	0.054	0.977	1.000	1.000
Ti(K)	72.339	47.110	0.349	0.985	1.299	1.000

Example 2. Spot was positioned close to the edge of the sample

Quantification Results at edge
Correction method: Thickness

Element	Weight %	Atomic %	Detector Uncertainty %	Absorption Correction	k-Factor	Correction
O(K)	31.868	58.274	0.675	0.514	1.980	1.000
Si(K)	0.258	0.268	0.064	0.977	1.000	1.000
Ti(K)	67.873	41.456	0.713	0.985	1.299	1.000

Background of sample H

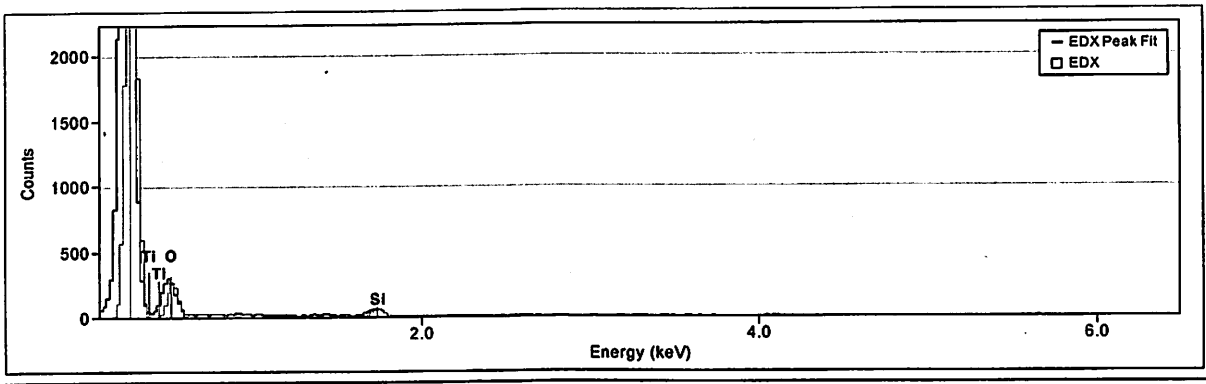

Quantification Results
Correction method: Thickness

Element	Weight %	Atomic %	Detector Uncertainty %	Absorption Correction	k-Factor	Correction
C(K)	97.760	98.401	0.861	0.173	6.279	1.000
O(K)	1.950	1.473	0.068	0.514	1.980	1.000
Si(K)	0.289	0.124	0.021	0.977	1.000	1.000

TiO_2 composition was confirmed. C, Cu, and Si in this sample came from copper grid covered with Lacey carbon. No measurable presence of other elements was detected in the sample.

Elemental composition of the sample was recalculated from original EDX data to exclude Si. Si was found in a background of the sample. Although it is possible that Si is present in the sample, it could not be distinguished from the background Si.

2. Elemental analysis by ICP

Ti = 59.40
Certified SPEX TiO_2 standard; Ti = 59.93%.
Theoretical titanium level in TiO_2; Ti = 59.95%.

The contaminants with the highest concentrations in the SPEX TiO_2 standard were: Co (753 ppm), P (25 ppm), SiO2 (538 ppm), and V (250 ppm).

Because the sample showed high purity, the ICP/MS system was set up to find contaminants, rather than directly measure the titania concentration. A complete set of thirty-one elements was checked, as shown in the master table for this analysis. The levels of contaminants in the highest concentration were: Al (896 ppm), As (707 ppm), Co (396 ppm), Na (218 ppm), SiO2 (496 ppm), V (121 ppm).

3. Specific surface area/porosity by BET

The BET surface area is 11.6 m^2/g, which would be equivalent to discrete primary particles of titania having an average diameter of 135 nm. This corresponds well to the average primary particle size estimated from TEM measurements of 214 nm (which would correspond to a surface area of 6.4 m^2/g).

Test/estimate	**Surface area, m^2/g**	**D_{av}, nm**
BET result, estimate of discrete primary particle size	**11.6**	135
D_{av} result, estimate of primary particle surface area	6.4	**214**

BET measurements of Sample H

Measurement	**PR-NC-08-10414**
BET, m^2/g	11.6
BJH adsorption cumulative surface area of pores, m^2/g	8.98 (0.85-150 nm)
BJH desorption cumulative surface area of pores, m^2/g	10.5 (0.85-150nm)
Single point surface area, m^2/g	10.9 (P/P_0=0.300)
BJH adsorption cumulative pore volume, cm^3/g	0.050
BJH desorption cumulative pore volume, cm^3/g	0.051
t-plot micropore area, m^2/g	0.60
t-plot external surface area, m^2/g	10.9
BJH adsorption pore diameter (4V/A), nm	11.0
BJH desorption pore diameter (4V/A), nm	9.7

4. Primary and aggregate size

TEM images show that most primary particles are ~200 nm in diameter. However, the distribution of primary particles is at least bimodal, as there are some nanoparticles with diameters near ~50 nm.

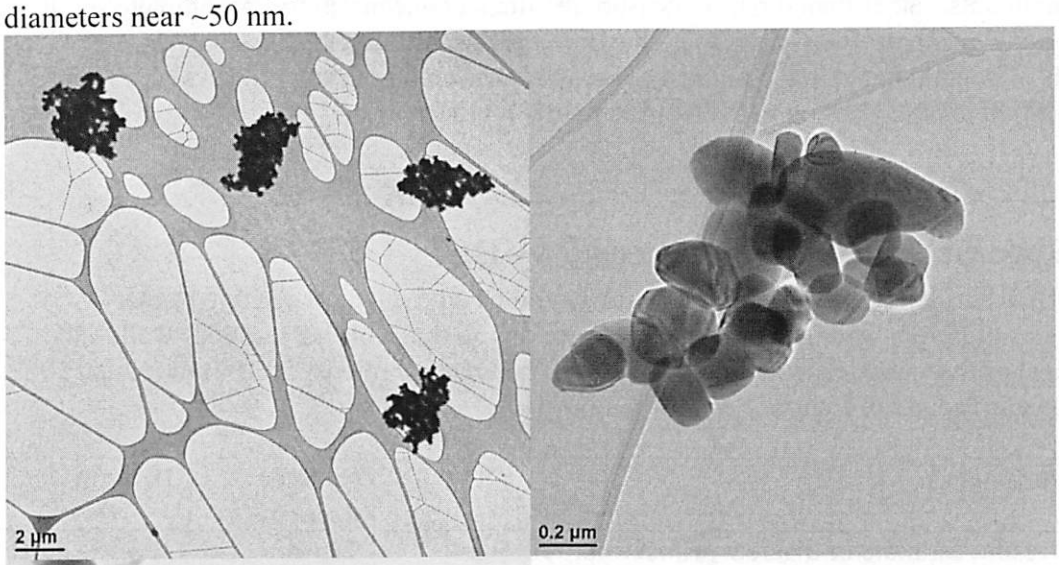

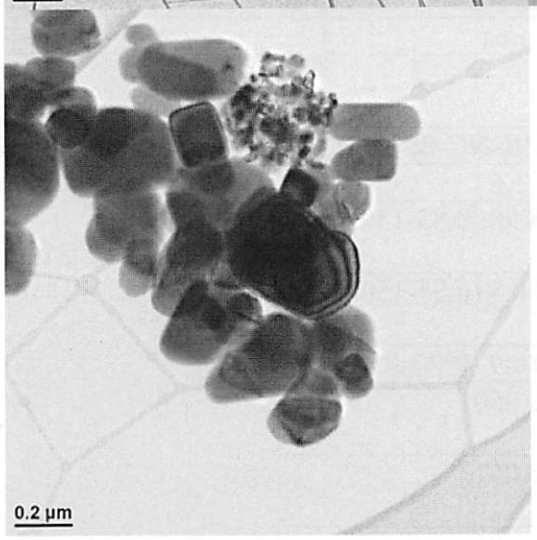

Image H1 a, b&c. Image H1a shows 2 µm aggregates. Image H1b shows typical aggregates in the submicron range. Image H1c shows an aggregate with a spherical cluster containing nanoparticles less than ~ 50 nm in diameter.

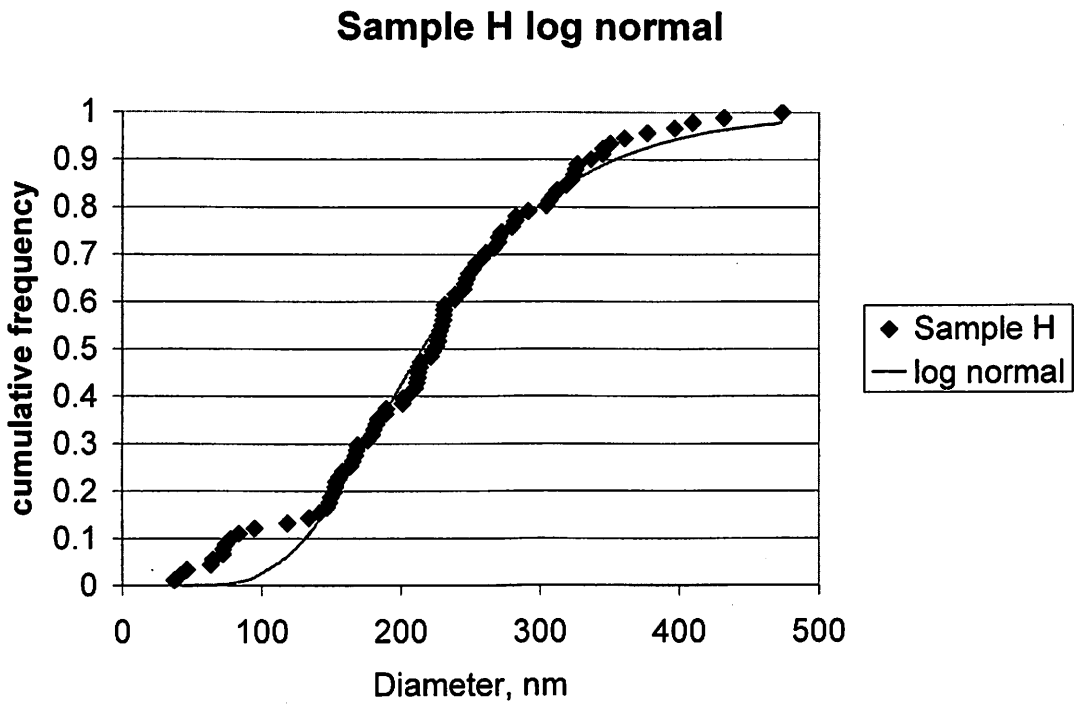

Log normal model parameters. Evaluation of TEM images gave the following table of the log normal distribution parameters that describe Sample D. The average particle size is 214 nm. The cluster containing small nanoparticles appears as a "step" for 50 nm < D < 100 nm on the cumulative frequency curve. The smaller nanoparticles are likely to cause an increase in the surface area measurement compared to the distribution average.

Log normal model coefficients

Coefficient	Estimate	Average standard error	Estimate/A.S.E.
Mean, lnμ [exp(μ) = 214 nm]	5.372	.005	1153
Standard dev., σ	0.387	0.008	46

Diameter range, 90% of sample fraction

	D_{05}, nm	Average diameter, nm	D_{95}, nm
Data	64	225	368
Model	114	214	409
Average size in small cluster		64	

5. Crystal structure by XRD

XRD pattern of the sample was matched with JCPDS card #21-1276 which correspond to rutile. The peaks are extremely narrow which indicates large primary size of the particles.

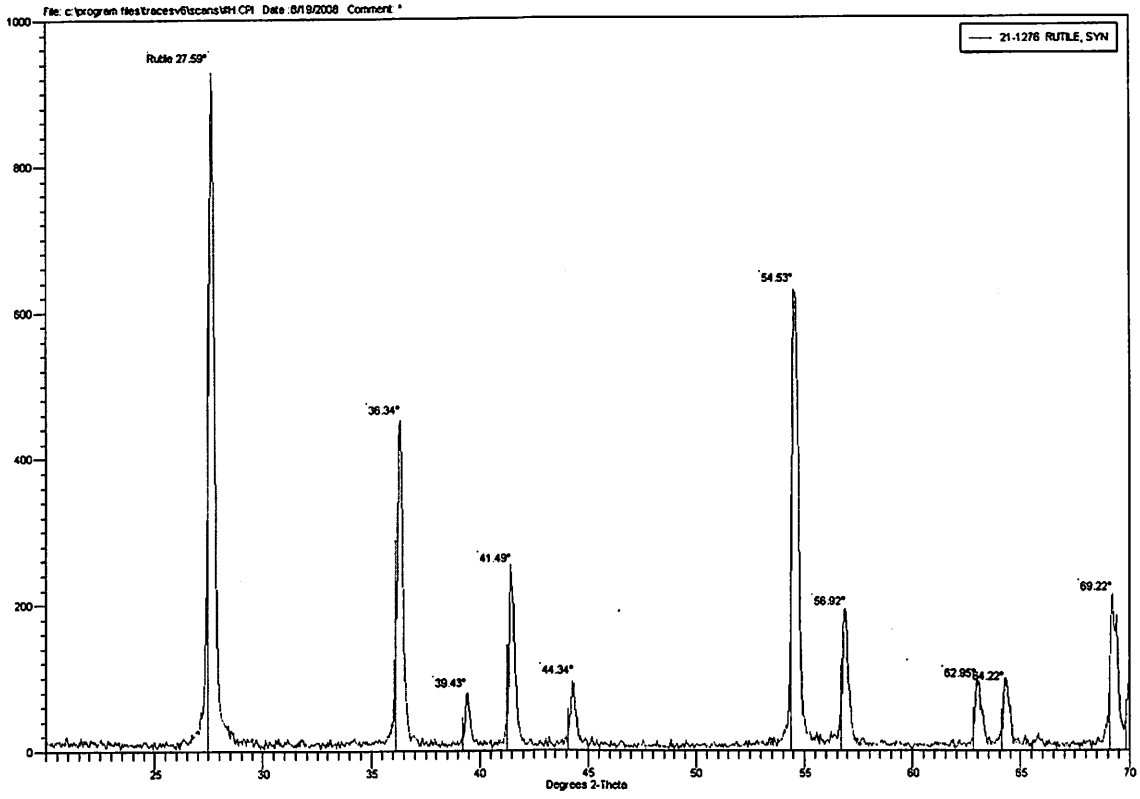

6. Elemental content

The elemental analysis results showed little carbon (< 0.05%), hydrogen (0.07%) and nitrogen (< 0.01%).

The elemental analysis of the SPEX titania standard was: carbon (< 0.05%), hydrogen (< 0.01%) and nitrogen (< 0.01%).

7. Particle shape and morphology

Table 7-1. Primary particle and aggregate sizes.

Method	Particle type	#	D_{av}, nm	Range, nm	Comments
TEM	Primary	91	214	37-410	Bimodal distribution
	aggregates		~1000		
DLS	1st peak;		~500		Appears to be near the

					primary particle average diameter
	2nd peak; aggregates	NA	~2000		Typical aggregate size
SEM	Primary		250-500		
	Aggregates		15-25 μm		

Sample ID	Sample H (Combined)
Operator ID	NM
Elapsed Time	00:05:00
Mean Diam.	466.8 nm
Rel. Var.	0.024
Skew	10.519

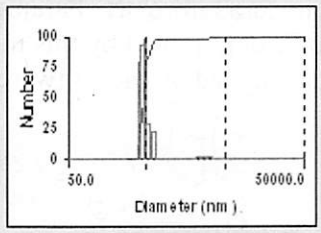

d(nm)	G(d)	C(d)	d(nm)	G(d)	C(d)	d(nm)	G(d)	C(d)
285.4	0	0	731.3	0	100	1874.2	0	100
310.9	0	0	796.7	0	100	2041.6	0	100
338.6	0	0	867.8	0	100	2223.9	0	100
368.9	0	0	945.3	0	100	2422.6	0	100
401.8	79	23	1029.8	0	100	2639.0	0	100
437.7	94	51	1121.7	0	100	2874.7	0	100
476.8	100	80	1221.9	0	100	3131.4	0	100
519.4	28	88	1331.1	0	100	3411.1	0	100
565.8	18	94	1449.9	0	100	3715.8	0	100
616.3	22	100	1579.4	0	100	4047.7	0	100
671.4	0	100	1720.5	0	100	4409.2	0	100

Number

SEM photos show aggregates in the range of 15-25 μm and primary particles near 400 nm.

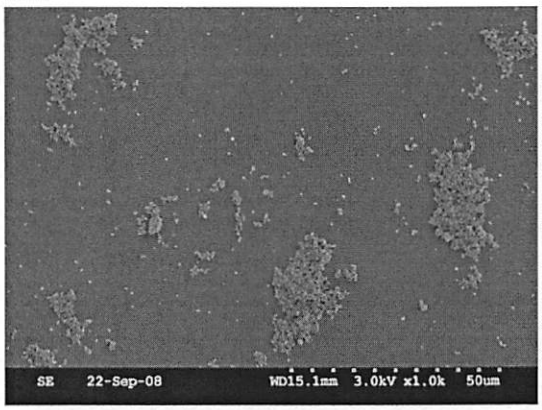

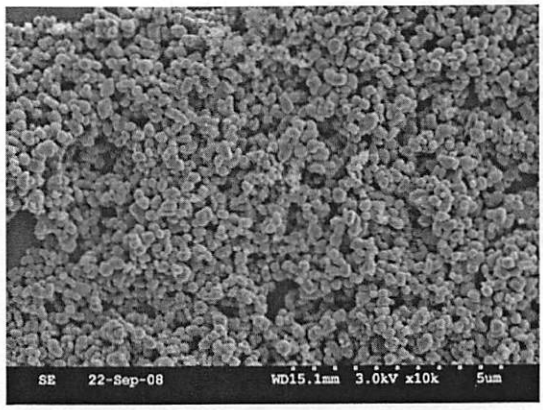

Appendix

H. Sample TiO_2, Mknano, Cat No. MKN-TiO2-R250, Lot No. 459/2007

4. Primary and aggregate size

Primary size of the particles was determined by using Digital Micrograph program from Gatan (files in .dm3 format). Parameters of only clearly visible and non-overlapping particle could be determined by this method. Each random qualified particle was outlined manually and analyzed by the software.

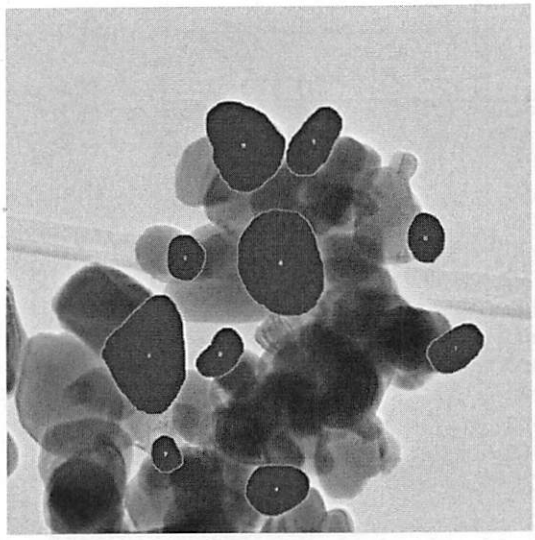

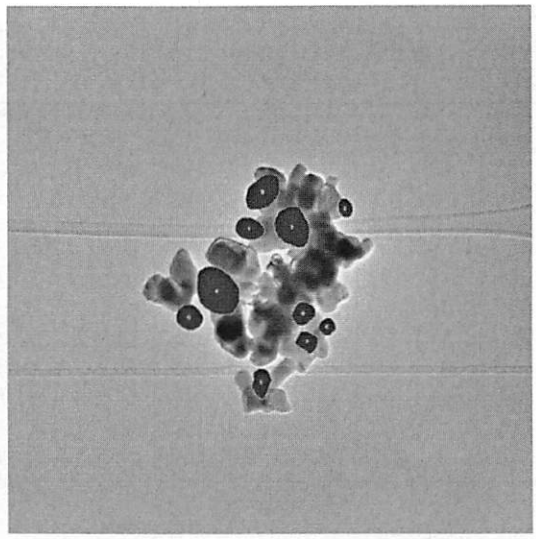

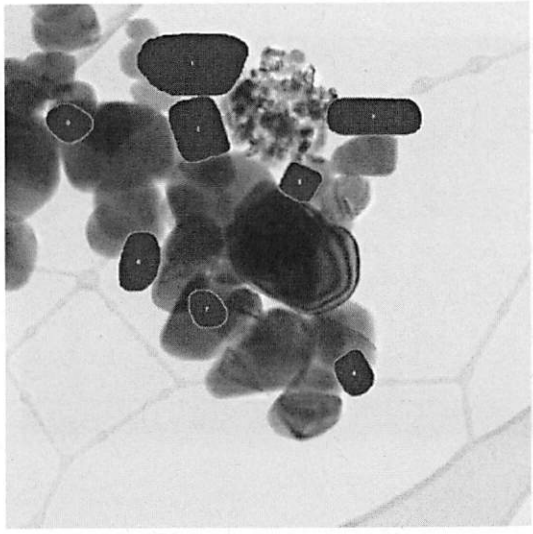

7. Particle shape and morphology

TEM images of the sample

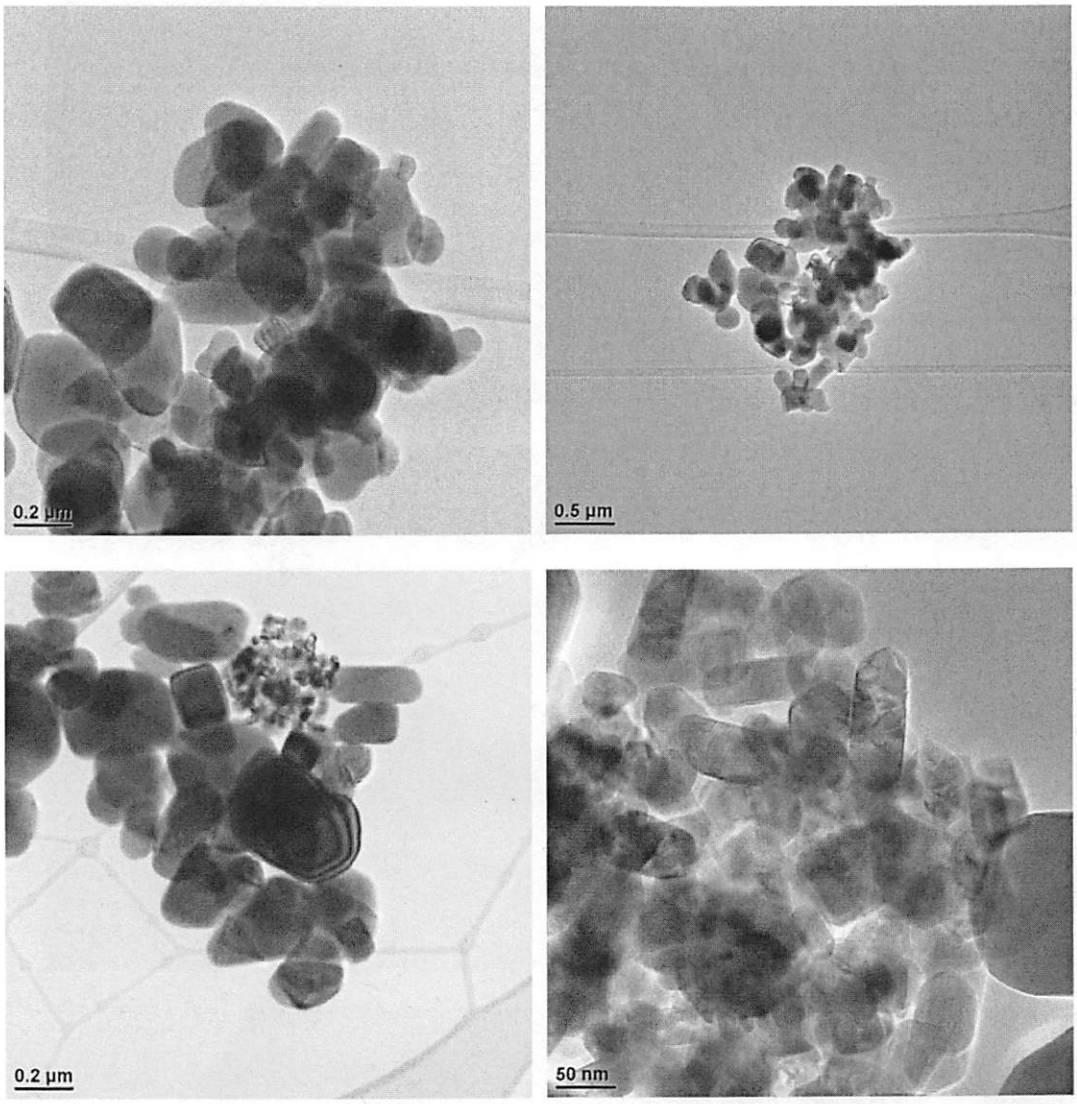

PR-NC-08-10414. Sample H.

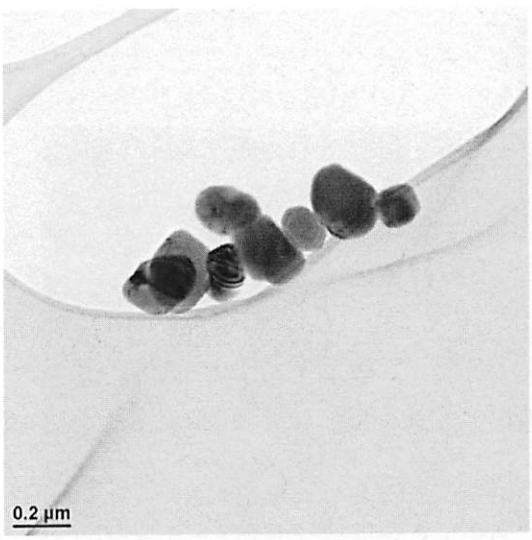

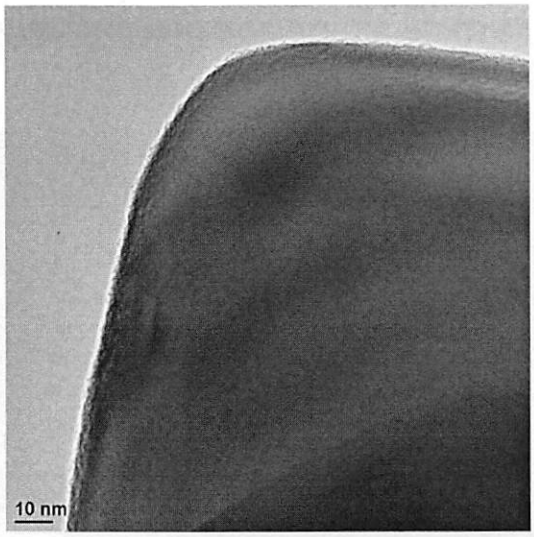

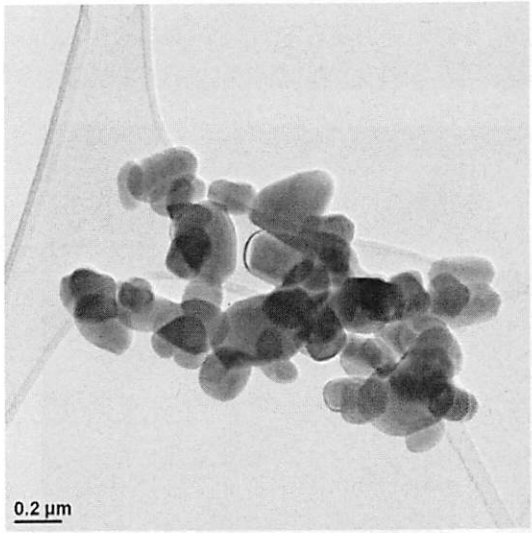

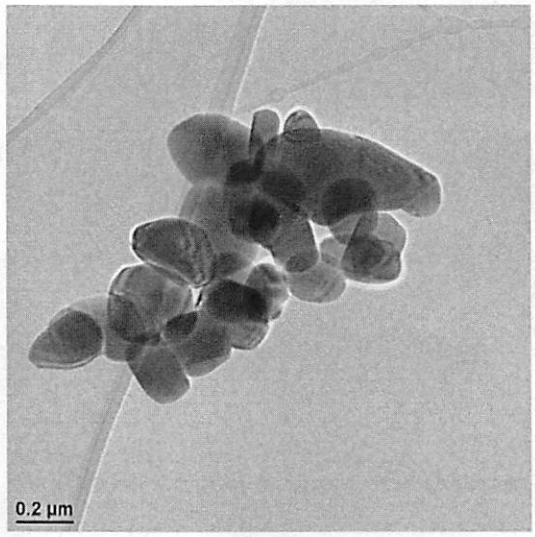

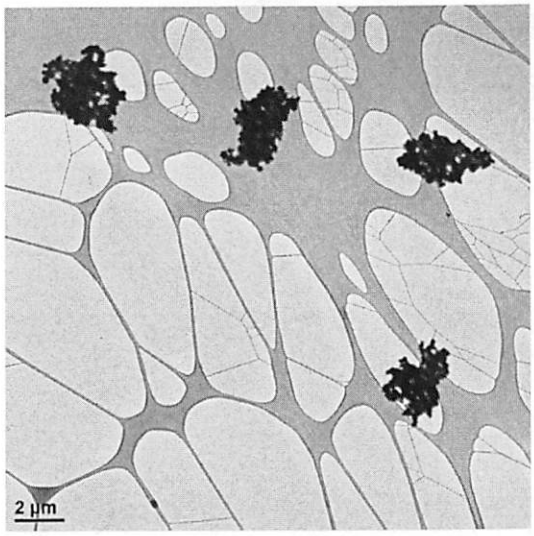

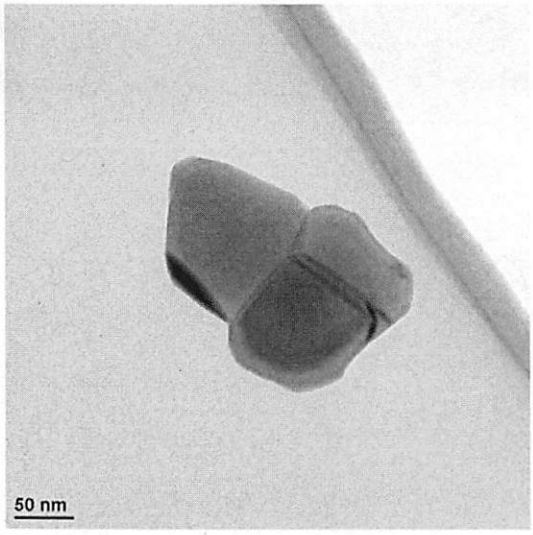

SEM images of the sample